Inclusive spectra of charged particles in pp and $\bar{p}p$ interactions at 32 GeV/c

E. E. Zabrodin* and L. V. Bravina*
Physics Department, University of Bergen, Allègaten 55, N-5007 Bergen, Norway

O. L. Kodolova, N. A. Kruglov, A. S. Proskuryakov, and L. I. Sarycheva
Institute of Nuclear Physics, Moscow State University, 119899 Moscow, Russia

M. Yu. Bogolubsky, M. S. Levitsky, V. V. Maksimov, A. A. Minaenko, A. M. Moiseev, and S. V. Chekulaev
Institute for High Energy Physics, 142284 Protvino, Russia
(Received 1 June 1994)

We present the inclusive and semi-inclusive spectra of charged particles in pp and $\bar{p}p$ interactions at an incident projectile momentum of 32 GeV/c, based on the full statistics of both experiments and obtained by means of the liquid hydrogen bubble chamber MIRABELLE at the Serpukhov accelerator. The spectra of charged particles are separated by a statistical method in the whole kinematically allowed region of phase space. Both inclusive and semi-inclusive cross sections of $\pi^{\pm}$, p, and K^- production in pp interactions are given. The differential cross sections are studied in terms of the Feynman variable x, rapidity, and transverse momentum. The results obtained strongly support the conclusion of the similarity of multiparticle production processes in pp and nonannihilation $\bar{p}p$ interactions. It is shown that the soft pp and $\bar{p}p$ interactions at the energies in question can be described at the quark-parton level in the framework of the quark-gluon string model. The derived particle spectra are compared with those at neighboring energies. The results of different phenomenological fits, including the hydrodynamical model predictions, are also listed.

PACS number(s): 13.75.Cs, 13.60.Hb, 12.40.Nn

I. INTRODUCTION

A great amount of experimental data have already provided important information about the processes of multiparticle production in high energy hadron-hadron interactions. But the investigation of soft hadronic collisions is still challenging due to the nonperturbative dynamics of interaction processes. The models describing soft interactions at the quark-parton level are intensively developed now and this helps to draw more definite conclusions concerning the dynamics of multiparticle formation in those interactions. We have compared data with the predictions of the quark-gluon string model (QGSM) [1,2], which seems to describe hadronic interactions rather well in a wide energy region. In particular, this model includes the $\bar{p}p$ annihilation process which plays a significant role at not very high energies, because its cross section falls as $s^{-1/2}$ with the energy increasing. As any other model, the QGSM contains a number of model-dependent parameters which have to be adjusted by comparison to experimental data. Unfortunately, the major part of the data was obtained in bare bubble chamber experiments (i.e., without identification of charged particles) by means of different chambers and of different processing methods. Sometimes the analysis of data was done for limited intervals of the space-time variables, which vary from one experiment to another.

The results on pp and $\bar{p}p$ interactions analyzed in this paper differ considerably from bubble chamber experiments at nearby energies. Their main methodological advantages are unique experimental conditions for both experiments, the same technique of data processing, detection and track measurements of both charged and neutral particles in a sufficiently large chamber volume, and an extensive statistics based on $\approx 250\,000$ fully measured $\bar{p}p$ interactions and $\approx 80\,000$ fully measured pp collisions.

The first two points are very important for the minimization of any influence of systematics on the compared data.

In this paper the new data on π^+, p, π^-, and K^- inclusive spectra in pp collisions at 32 GeV/c are presented for the reactions

$$pp \rightarrow p + X, \quad (1)$$
$$pp \rightarrow \pi^+ + X, \quad (2)$$
$$pp \rightarrow \pi^- + X, \quad (3)$$
$$pp \rightarrow K^- + X, \quad (4)$$

as well as data on the corresponding semi-inclusive spectra for the whole kinematically allowed region of phase space. These data are compared with inclusive and semi-inclusive π^+, π^-, p, $\bar{p}$ spectra in $\bar{p}p$ interactions at the same energy. A detailed investigation of the inclusive production of $\pi^{\pm}$'s and protons in $\bar{p}p$ interactions at 32 GeV/c based on a part of the statistics ($\approx 55\,000$ events) was done in [3]. Some preliminary data on the reactions (1)–(4) based on a partial statistics ($\approx 35\,000$ events)

*On leave from Institute of Nuclear Physics, Moscow State University, Moscow, Russia.

were already reported in [4].

The paper is organized as follows. A brief description of the data handling process is given in Sec. II. Sec. III is devoted to the problems of a statistical separation of charged particle spectra and Sec. IV explains the main differences between pp and $\bar{p}p$ interactions from the QGSM point of view. In Sec. V, average multiplicities and inclusive cross sections of charged particles are listed for both experiments. Semi-inclusive and inclusive differential distributions of particle production, as well as the results of phenomenological fits, are shown in Sec. VI. Section VII contains the study of the properties of transverse momentum distributions of secondary hadrons, which are among the most direct manifestations of hadronic interaction dynamics and so are one of the crucial tests for models of soft hadron-hadron interactions.

Of particular interest in $\bar{p}p$ collisions is the annihilation process, when one has only $(q\bar{q})$ meson systems in the final state. Several theories use the assumption that the differences between pp and $\bar{p}p$ interactions arise mainly due to annihilation. Therefore, Sec. VIII is concerned with the comparison of pp interactions to non-annihilation $\bar{p}p$ collisions.

In the Appendix a statistical method of deriving charged particle spectra is described in detail. Final results are summarized in the Conclusions.

II. EXPERIMENTAL DETAILS

The experimental data come from about 300 000 and 100 000 frames of an exposure of the MIRABELLE chamber to antiprotons and protons, respectively. All frames were scanned twice for events of all topologies. These results were then checked in a third scan. The cross sections σ_n for the various charged particle multiplicities n were determined from this scanning procedure [5]. After the third scan all events were measured by means of precise semiautomatic measuring projectors and the results of the measurements were reconstructed by the geometrical reconstruction program H-GEOM. Events for which this program failed to reconstruct all charged tracks correctly were measured twice. The average passing rates were not less than 90% for the two- and four-prong topologies and about 70–75 % for more complex topologies.

For physics analysis we selected only completely reconstructed events, for which all track momenta were determined with a precision better than 25%, i.e., $\Delta P/P < 0.25$. All losses of events at the production step were thoroughly compensated for by topology-dependent weights. Slow protons (with $P_{\rm lab} < 1.2$ GeV/c) were identified on the basis of the ionization density of tracks. Kinematic fitting of all events was done by GRIND or, for part of the pp statistics, by H-KINEMATICS programs. Elastic collisions were excluded from the analysis.

The details of the processing of the experimental data can be found in [6–8] and references therein.

III. SEPARATION OF PARTICLE SPECTRA

It is not sufficient to know the laboratory momenta of tracks to obtain the correct phase-space distributions for charged particles in reactions (1)–(4) as from a bare bubble chamber experiment; one has to know also their masses. For pp interactions, the positively charged secondaries consist of protons and pions with a small admixture of kaons ($\sim$ 5%) and a negligibly small admixture of positrons. The spectrum of negative particles consists mainly of pions with a small fraction of kaons and electrons. As mentioned above, it is possible to separate protons with $P_{\rm lab} < 1.2$ GeV/c by ionization. This covers only a small region of phase space, and so the separation of charged particles cannot be performed for individual events. In order to yield the individual spectra one has to use statistical methods, which are valid for the whole sample of events but not for a single event. Forward-backward symmetry of the particle spectra in the center-of-mass system (c.m.s.) is expected due to the initial symmetry of the pp system. This allows one to separate p, π^+, π^-, and K^- statistically, using the mass dependence of the Lorentz transformation of their momentum from the laboratory (target) system to the projectile system and vice versa. Because of the charge conjugation symmetry of $\bar{p}p$ collisions, practically the same statistical separation procedure can be applied for particle spectra in these interactions.

A number of similar statistical algorithms is described in the scientific literature for pp interactions [9–12], as well as their modifications for $\bar{p}p$ interactions [13–15]. As usual, these methods provide the separation of p, π^+, π^- spectra for pp interactions, and the separation of $p, \pi^+, \pi^-, \bar{p}$ spectra for $\bar{p}p$ collisions. Kaons are not included in the symmetrization procedure. Figure 1 shows the violation of forward-backward symmetry for negatively charged particles, produced in pp interactions, when all are assumed to be π^-'s. Evidently, it is nec-

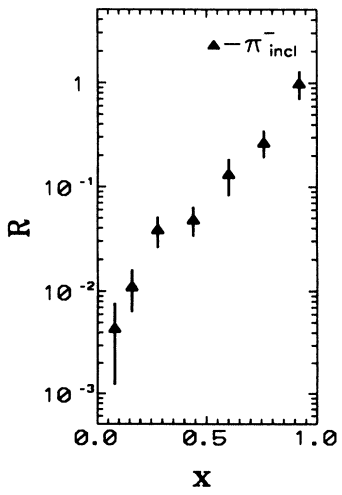

FIG. 1. Forward-backward asymmetry $R = |F_B(x) - F_F(x)|/[F_B(x) + F_F(x)]$ for negatively charged particles in pp interactions. All particles are assumed to be π^-'s.

essary to take into account kaon contamination at our energies, even in order to provide more accurate results for π^-'s. A method to separate $K^\pm$ spectra was proposed in [3] for $\bar{p}p$ interactions. This method is rather complicated and there is no rigorous mathematical proof of its correctness. So a modified method was used. Its basic ideas are presented in [11] (pp interactions) and in [14,15] ($\bar{p}p$ interactions). The full mathematical description of the procedure including its generalization to the separation of $K^\pm$ spectra is given in the Appendix. These ideas for $K^\pm$ separation were first formulated in [4].

After a thorough analysis of the method on Monte Carlo–simulated spectra and on spectra obtained from fitted exclusive reactions, this method was applied to the full statistics of both experiments.

IV. MODEL FOR THE DESCRIPTION OF HADRONIC INTERACTIONS AT HIGH ENERGIES (QGSM)

In order to compare large amounts of experimental data with theoretical ideas numerous programs exist to generate hadronic and nuclear collisions at high energies. The most widely used programs are those from the Lund University, in particular PYTHIA [16] and FRITIOF [17]. It is claimed that these programs describe the entire range of momentum transfer Q^2, from hard quark and gluon scattering to hadron production and decay, which explains their popularity. However, in proton-antiproton collisions at momenta up to ~ 100 GeV/c an important contribution to the interaction cross section comes from the $\bar{p}p$ annihilation process, a leading factor in the difference between the inclusive characteristics of pp and $\bar{p}p$ interactions. It must be taken into account in any model simulations of $\bar{p}p$ interactions. Since it is not included in the programs mentioned above, we used the QGSM [1,2] for comparison with the experimental data. The QGSM is based on the so-called QCD $1/N$ series expansion [19] of the amplitude for processes in QCD and on string-type phenomenological models describing the quark transitions into hadrons. When the amplitude for hadronic processes is expanded in $1/N$, diagrams of various topologies arise. At high energies, these diagrams correspond to processes with the exchange of Regge singularities in the t channel. For instance, *planar* diagrams correspond to the exchange of secondary Reggeons, and *cylindrical* diagrams correspond to Pomeranchuk poles in classic scattering. The QGSM is similar to the dual parton model (see [20,21] and references therein), yet it uses structure functions based on the asymptotics obtained in Regge theory. Together with the annihilation process, the model contains also the process of diffraction dissociation of the incident and target particles with small mass excitation (corresponding to the triple-Reggeon limit) and diffraction with large-mass excitation (corresponding to the triple-Pomeron limit).

Figure 2 shows the variety of particle production subprocesses taken into account in the current version of the QGSM [2,18] for pp and $\bar{p}p$ interactions.

The inelastic cross sections are

$$\sigma_{\rm in}^{pp}(s) = \sigma^P(s) + \sigma^{\rm uncyl}(s) + \sigma^{\rm rear}(s) + \sigma^{\rm dif}(s) + \sigma^{\rm reg}(s), \tag{5}$$

$$\sigma_{\rm in}^{\bar{p}p}(s) = \sigma^P(s) + \sigma^{\rm uncyl}(s) + \sigma^{\rm plan}(s) + \sigma^{\rm dif}(s) + \sigma^{\rm reg}(s) + \sigma^{\rm ann}(s), \tag{6}$$

where $\sigma^P(s)$ is the cross section for the multichain processes described by the cylindrical diagram and diagrams with multi-Pomeron scattering [Fig. 2(b)], $\sigma^{\rm uncyl}(s)$ by the undeveloped cylinder diagram [Fig. 2(c)], $\sigma^{\rm plan}(s)$ by the planar diagram [Fig. 2(a)], $\sigma^{\rm rear}(s)$ by the diagram with rearrangement of quarks [Fig. 2(d)], $\sigma^{\rm dif}(s)$ by the diffraction processes [Fig. 2(e), 2(f)], $\sigma^{\rm ann}(s)$ by the annihilation diagrams [Fig. 2(g), 2(h), 2(i)], and $\sigma^{\rm reg}(s)$ by the triple-Reggeon diagram [Fig. 2(k)].

The total interaction cross sections, the elastic cross sections, and the cross sections for one-vertex and double diffractive dissociation were taken from the experimental data with quadratic interpolation at intermediate energy [2]. The other cross sections were calculated using the energy dependences obtained in the Regge approach [22].

A specific feature of this model as a string-type model is that particles are produced through the formation and breakup of quark-gluon strings—excited objects which consist of quarks connected by a gluon string. The string breakup procedure is based on the Field-Feynman algorithm [23] and includes the conservation of energy, momentum, and quantum numbers of the string and the conversion of quarks into hadrons.

Comparison with the wide spectrum of experimental data at momenta from 12 to 100 GeV/c shows [2,18] that the QGSM successfully reproduces the multiplicity distributions and the inclusive spectra of particles of different origin in $\bar{p}p$ and pp interactions. The analysis of the multiplicity distributions shows that different diagrams contribute to different regions of $n_\pm$. In particular, including the process with multiple string production makes it

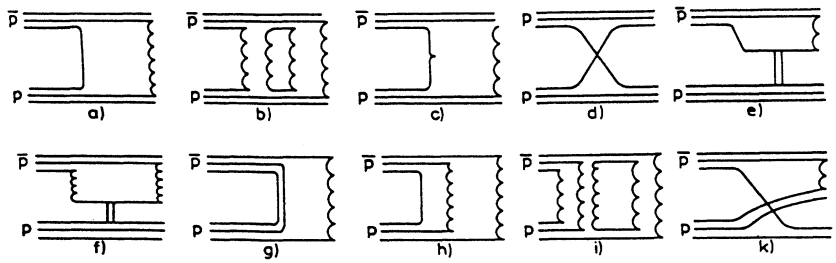

FIG. 2. Diagrams of the processes in the inelastic $\bar{p}p$ and pp interactions. The description of the diagrams is given in the text.

possible to describe the multiplicity distribution in the region with high $n_{\pm}$ [18].

V. INCLUSIVE CROSS SECTIONS AND AVERAGE MULTIPLICITIES OF THE CHARGED PARTICLES

The reconstruction of the inclusive charged particle spectra in the whole kinematically allowed region of phase space permits one to calculate some important average production characteristics of the secondaries, both in pp and $\bar{p}p$ interactions at 32 GeV/c.

The values of the inclusive cross sections of protons and π^+ mesons are listed in Table I. All data are normalized to the topological cross sections in pp and $\bar{p}p$ collisions at 32 GeV/c from [5,24]. Within the error bars the data for $\bar{p}p$ interactions coincide with the same data obtained in [3].

The inclusive and semi-inclusive cross sections of π^- and K^- mesons are given in Table II.

Using the definition of average multiplicities of each type of particle $\langle n^i \rangle_{n_{\rm ch}}$,

$$\langle n^i \rangle_{n_{\rm ch}} = \frac{1}{\sigma_{\rm incl}} \int \frac{d^3\sigma_{n^i_{\rm ch}}}{dp} dp, \qquad (7)$$

where $i = p, \pi^+, \pi^-, K^-$, and $\sigma_{\rm incl}$ means the topological inelastic cross section, we present the values of $\langle n^i \rangle_{n_{\rm ch}}$ for $\pi^{\pm}$ and K^- mesons in pp interactions at 32 GeV/c in Table III.

The values of $\langle n^p \rangle_{n_{\rm ch}}$ obtained in pp interactions at the projectile momenta 24 GeV/c [9], 32 GeV/c, and 69 GeV/c [12], respectively, are given in Table IV. From this table one can conclude that the proton topological multiplicities for pp collisions at 32 GeV/c are closer to those at 69 GeV/c than at 24 GeV/c. The average multiplicity of protons ($\langle n^p \rangle_{n_{\rm ch}} = 1.20 \pm 0.03$ at 32 GeV/c) shows no increase within the interval from 24 GeV/c up to about 100 GeV/c of projectile momenta, and the difference between the average multiplicities of π^+ and π^- mesons (0.85±0.05 at 32 GeV/c) decreases with the rise of energy (Fig. 3). A detailed investigation of the moments of the inelastic charged particle multiplicity distributions for pp and $\bar{p}p$ interactions at 32 GeV/c was done in [5].

Comparison of the average proton multiplicities in pp and $\bar{p}p$ experiments at 32 GeV/c (Fig. 4) demonstrates that in pp interactions $\langle n^p \rangle_{n_{\rm ch}}$ increases with increasing multiplicity $n_{\rm ch}$ up to the ten-prong topology and then falls, while it drops for $n_{\rm ch} \geq 6$ in $\bar{p}p$ collisions. This circumstance is connected to the $\bar{p}p$ annihilation process, which contributes mainly to the more complex topologies. Values for $\langle n^p \rangle_{n_{\rm ch}}$ in pp and $\bar{p}p$ interactions at 8.8 GeV/c were calculated from the data of [25]. They show the beginning of a significant divergence in average proton multiplicities already for two-prong events. It is important to note here that one has to take 1/2 of $\langle n^p(pp) \rangle$ values for the comparison.

It was mentioned in several articles, e.g., in [15], that, under the assumption of the equality of topological nonannihilation cross sections in $\bar{p}p$ interactions to the corresponding cross sections in pp interactions, the mean multiplicities of protons for different topologies in pp and nonannihilation $\bar{p}p$ interactions coincide within errors. One of the goals of this further investigation is to compare inclusive and semi-inclusive proton production in both experiments in order to test the validity of this assumption at 32 GeV/c.

TABLE I. Inclusive and semi-inclusive cross sections σ_i (mb), $i = \pi^+$, p, and n_c^+ for pp and $\bar{p}p$ interactions at 32 GeV/c. Of each pair of numbers, the upper one is for pp and the lower one is for $\bar{p}p$ interactions.

Multiplicity	$\sigma^p_{n_c}$ (mb)	$\sigma^{\pi^\pm}_{n_c}$ (mb)	$\sigma^+_{n_c}$ (mb)
2 prong	7.82 ± 0.5	7.20± 0.5	14.94 ±0.45
inelastic	3.56 ± 0.4	3.80± 0.4	7.36 ±0.30
4 pr.	13.50 ± 0.5	20.40± 0.6	33.96 ±0.50
	7.33 ± 0.4	17.55± 0.4	25.14 ±0.40
6 pr.	9.88 ± 0.4	20.98± 0.4	30.96 ±0.40
	5.38 ± 0.4	23.16± 0.4	28.56 ±0.40
8 pr.	4.34 ± 0.4	11.76± 0.4	16.10 ±0.40
	2.24 ± 0.4	17.25± 0.4	19.44 ±0.35
10 pr.	1.41 ± 0.2	4.10± 0.3	5.52 ±0.25
	0.60 ± 0.2	8.80± 0.3	9.41 ±0.20
12 pr.	0.21 ± 0.03	0.97± 0.08	1.20 ±0.08
	0.06 ± 0.05	2.98± 0.05	9.41 ±0.05
14 pr.	0.03 ± 0.005	0.20± 0.02	0.24 ±0.03
	0.056± 0.03	0.706± 0.03	0.76 ±0.04
16 pr.	0.003± 0.001	0.02± 0.009	0.027±0.01
	-	0.127± 0.02	0.13 ±0.02
All	37.20 ± 2.0	65.63± 2.1	102.95 ±2.10
	19.22 ± 1.8	74.37± 1.8	93.80 ±1.80

TABLE II. Inclusive and semi-inclusive cross sections σ_i (mb), $i = \pi^-$, K^- and n_c^- for pp interactions at 32 GeV/c.

Multiplicity	$\sigma^{\pi^-}_{n_c}$ (mb)	$\sigma^{K^-}_{n_c}$ (mb)	$\sigma^-_{n_c}$ (mb)
4 prong	10.63±0.25	0.667±0.25	11.32±0.20
6 pr.	14.85±0.35	0.581±0.35	15.48±0.30
8 pr.	9.43±0.30	0.213±0.30	9.66±0.25
10 pr.	3.59±0.10	0.095±0.10	3.70±0.16
≥ 12 pr.	1.02±0.05	0.027±0.05	1.06±0.10
All	39.52±0.30	1.580±0.30	41.22±0.40

TABLE III. Average inclusive and semi-inclusive multiplicities for $\pi^{\pm}$ and K^- mesons in pp interactions at 32 GeV/c.

Multiplicity	$\langle n^{\pi^+} \rangle_{n_c}$	$\langle n^{\pi^-} \rangle_{n_c}$	$\langle n^{K^-} \rangle_{n_c}$
2 pr. inel.	0.96 ± 0.06	-	-
4 pr.	1.80 ± 0.05	0.94± 0.04	0.060±0.02
6 pr.	2.71 ± 0.05	1.92± 0.04	0.075±0.02
8 pr.	3.65 ± 0.08	2.93± 0.05	0.066±0.03
10 pr.	4.46 ± 0.15	3.90± 0.10	0.101±0.05
≥ 12 pr.	5.67 ± 0.30	4.85± 0.20	1.145±0.69
All	2.13 ± 0.03	1.28± 0.02	0.050±0.015

TABLE IV. Average inclusive and semi-inclusive multiplicities for protons in pp interactions at 24, 32, and 69 GeV/c.

Multiplicity	$\langle n^p \rangle_{n_c}$		
	24 GeV/c	32 GeV/c	69 GeV/c
2 pr. inel.	1.050± 0.040	1.047± 0.06	1.06 ±0.03
4 pr.	1.278± 0.012	1.20± 0.05	1.17 ±0.03
6 pr.	1.328± 0.017	1.27± 0.05	1.22 ±0.04
8 pr.	1.429± 0.033	1.34± 0.09	1.35 ±0.09
10 pr.	1.481± 0.100	1.53± 0.15	1.35 ±0.09
$\geq$ 12 pr.	-	1.23± 0.30	1.26 ±0.13
All	1.24 ± 0.03	1.20± 0.03	1.22 ±0.02

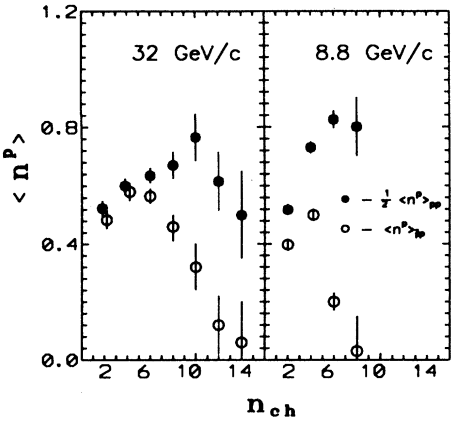

FIG. 4. The multiplicity dependence of the average number of protons for inelastic events in pp and $\bar{p}p$ interactions at 32 and 8.8 GeV/c. Open circles, $\langle n^p \rangle$ in $\bar{p}p$ interactions; solid circles, $1/2\langle n^p \rangle$ in pp interactions.

VI. DIFFERENTIAL CROSS SECTIONS OF INCLUSIVE PRODUCTION OF CHARGED PARTICLES

A. Inclusive distributions

In this section, the inclusive single-particle spectra are analyzed in terms of the following kinematic variables:

Feynman variable $x_F = \dfrac{2P_{||}^{\text{c.m.}}}{\sqrt{s}}$,

rapidity $y = \frac{1}{2}\ln\dfrac{E+P_{||}}{E-P_{||}} = \operatorname{arctanh}\left(\dfrac{P_{||}}{E}\right)$,

and squared transverse momentum P_T^2.

It is well known that the Lorentz-invariant differential cross section $E\frac{d^3\sigma}{dp}$ depends only on three variables: the total energy $\sqrt{s}$ of the final state in the c.m.s., the transverse component of the momentum vector, and one of the variables (x_F or y) dealing with the particle's longitudinal momentum. So for unpolarized beams

$$E\frac{d^3\sigma}{dp} = \frac{1}{\pi}\frac{d^2\sigma}{dy\,dP_T^2} = \frac{2E^*}{\pi\sqrt{s}}\frac{d^2\sigma}{dx\,dP_T^2} \ . \tag{8}$$

From hereon we shall use an asterisk to indicate c.m.s. quantities. Thus, the invariant distributions usually introduced for the physical interpretation of the data will be the invariant x distribution ($x \equiv x_F$)

$$F(x) = \frac{2}{\pi\sqrt{s}}\int E^*\frac{d^2\sigma}{dx\,dP_T^2}dP_T^2 \ , \tag{9}$$

the double differential invariant cross section

$$F(x,P_T^2) = \frac{2}{\pi\sqrt{s}}\int_{P_{T_1}^2}^{P_{T_2}^2} E^*\frac{d^2\sigma}{dx\,dP_T^2}dP_T^2 \ , \tag{10}$$

and the c.m.s. rapidity distribution

$$\frac{d\sigma}{dy^*} = \int \frac{d^2\sigma}{dy^* dP_T^2}dP_T^2 \ . \tag{11}$$

Because of the forward-backward symmetry of pp interactions, all longitudinal distributions are symmetric about $x = y^* = 0$, which corresponds to $y_{\text{lab}} = 2.2$.

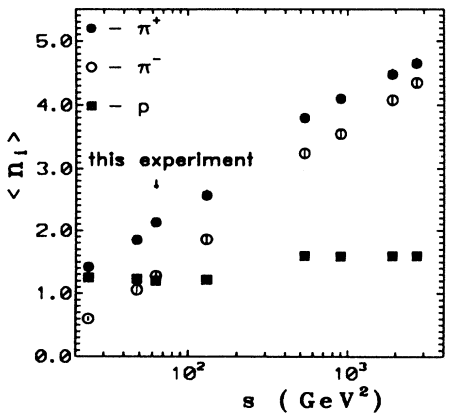

FIG. 3. The energy dependence of the average number of protons and pions for inelastic pp interactions.

B. Proton production

If not specifically mentioned, we shall compare the proton spectra in pp interactions to the combined proton+antiproton spectra in $\bar{p}p$ interactions in order to avoid any differences in the central ($|x| \leq 0.25$) region.

Figure 5 shows the inclusive and semi-inclusive $d\sigma/dx$ distributions of proton and combined $p+\bar{p}$ spectra in pp and $\bar{p}p$ interactions, respectively. The diffractive dissociation gives a significant contribution for two- and four-prong events only. For larger multiplicities these distributions become more central. The proton spectra in pp collisions and the combined spectra in $\bar{p}p$ interactions coincide within errors. The histograms shown in this figure correspond to the predictions of the QGSM for both interactions.

The inclusive and semi-inclusive invariant x distributions $F(x)$ are presented in Fig. 6 for the proton and combined spectra. The solid line histogram denotes the

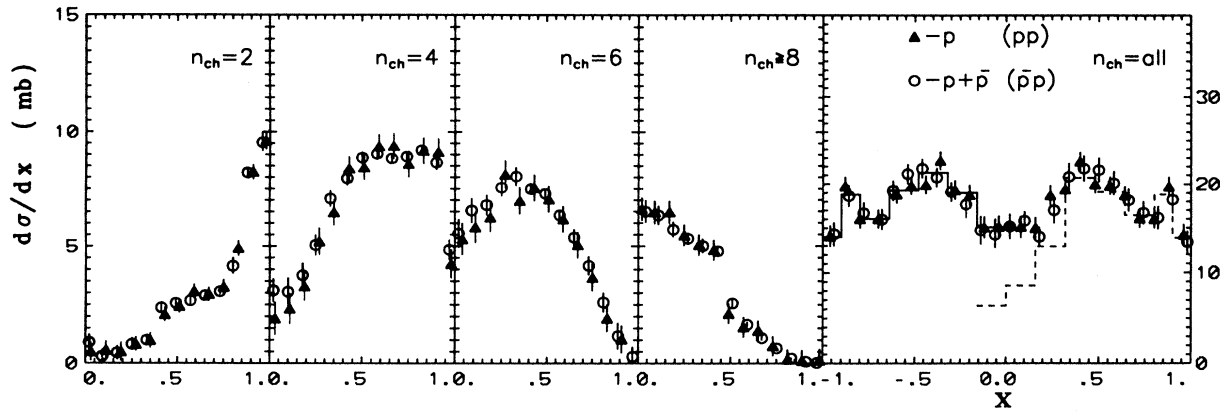

FIG. 5. Semi-inclusive and inclusive $d\sigma/dx$ distributions of p and $p+\bar{p}$ in pp and $\bar{p}p$ interactions at 32 GeV/c. The solid-line histogram corresponds to the QGSM predictions for protons (backward hemisphere) in pp collisions and the dashed one corresponds to the QGSM predictions for antiprotons (forward hemisphere) in $\bar{p}p$ interactions.

predictions of the QGSM for the $p+\bar{p}$ spectrum in $\bar{p}p$ interactions. The discrepancies between the model results and the experimental data lie within the limit of 10% accuracy, and so the QGSM successfully approximates both pp and $\bar{p}p$ soft interactions, although the sets of the diagrams of subprocesses, involved in the model for the description of pp and $\bar{p}p$ interactions, are not the same (Fig. 2).

For the investigation of the particle energy dependence of the p and $\bar{p}$ spectra the invariant double differential cross section $F_p(x, P_T^2)$ is shown for protons and antiprotons in the backward hemisphere in Fig. 7, as a function of x for several intervals of P_T^2. It is apparent that both distributions have similar shapes in any P_T^2 interval, except the central region at high P_T^2, where $F_p^{pp}(x, P_T^2)$ seems to be smaller than that in $\bar{p}p$ interactions.

The inclusive and semi-inclusive $d\sigma/dy^*$ distributions for protons in both experiments are shown in Fig. 8. One can see again that these spectra are similar. The inclusive y^* distribution of protons in pp collisions is also given in Fig. 9 with those at 24 GeV/c and 69 GeV/c. The histograms are the predictions of the QGSM. This comparison shows that in the central region all of the distributions fall with decreasing y^* approximately at the same rate, and, for $y^* = 0$,

$$\frac{d\sigma}{dy^*} = 4.6 \pm 0.2 \text{ mb} . \tag{12}$$

Near the proton fragmentation region the distribution at 32 GeV/c is closer to that at 24 GeV/c than to that at 69 GeV/c, although a local minimum at $y^* = 1.7$ becomes distinguishable. The direct investigation of a part of the nonannihilation process in $\bar{p}p$ interactions at 32 GeV/c and its comparison with the pp data will be performed in a separate section below, but from the various inclusive and semi-inclusive spectra presented the following conclusion can be drawn: The inclusive proton spectra in pp interactions and the combined $\bar{p}+p$ spectra in $\bar{p}p$ collisions coincide within the accuracy of the data at 32 GeV/c. According to the QGSM, the processes responsible for $\bar{p}+p$ production in pp and $\bar{p}p$ collisions are different (see Fig. 2). It means that the contribution of the planar diagram [Fig. 2(a)] in $\bar{p}p$ interactions at this energy is small.

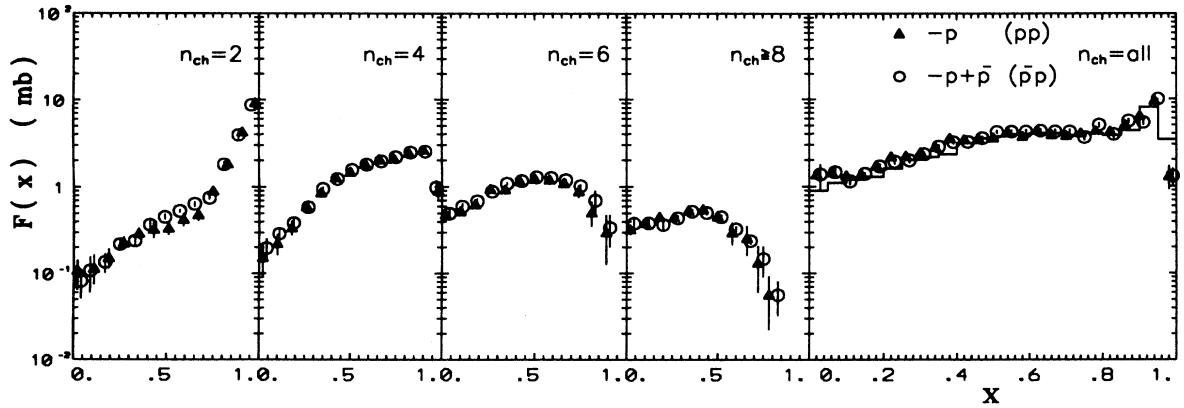

FIG. 6. Semi-inclusive and inclusive invariant x distributions of p and $p+\bar{p}$ in pp and $\bar{p}p$ interactions at 32 GeV/c. The histogram corresponds to the QGSM predictions of the $\bar{p}$ spectrum in $\bar{p}p$ interactions.

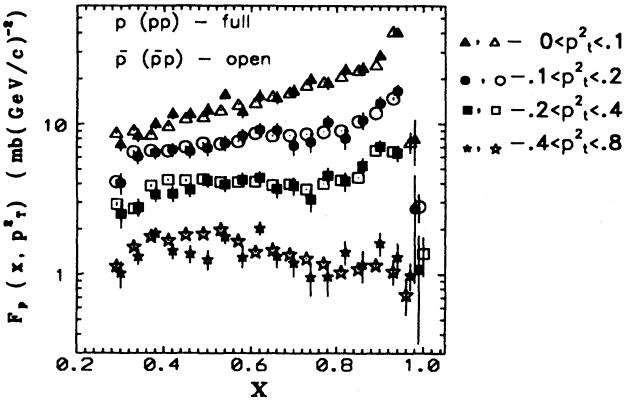

FIG. 7. Double differential invariant cross sections of protons (pp, solid symbols) and antiprotons ($\bar{p}p$, open symbols) as a function of x for individual P_T^2 intervals.

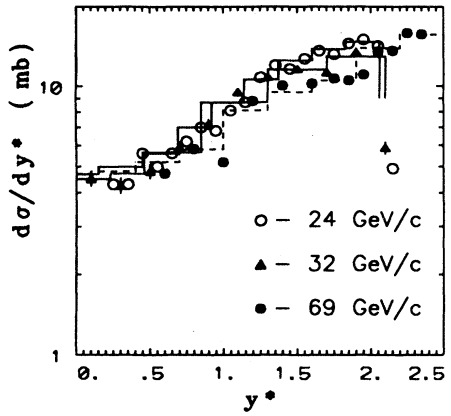

FIG. 9. Rapidity distributions of protons in pp interactions at 24, 32, and 69 GeV/c. Histograms denote the QGSM predictions.

C. Differential distributions of $\pi^{\pm}$ mesons

Figures 10, 11, and 12 present inclusive and semi-inclusive invariant x distributions $F(x)$ of π^+ and π^- mesons in pp interactions, together with the corresponding distributions of π^+ mesons in $\bar{p}p$ interactions at 32 GeV/c. The curves projected onto the inclusive distributions correspond to the results of a fit by the function

$$\frac{d\sigma}{dx} = A\,(1-|x|)^n \qquad (13)$$

for $-0.7 \le x \le -0.2$. The results of the fits are listed in Table V for π^+'s in pp and $\bar{p}p$ interactions and in Table VI for π^-'s in pp interactions. In the dimensional counting rule (DCR) [26] the fragmentation power of $(1-|x|)$ in (13) is connected with the (i) vector-gluon exchange and (ii) quark exchange or annihilation. For instance, the DCR predicts [26] that for $p \xrightarrow{p/\bar{p}} \pi^+$ fragmentation $n = 3$ for the quark exchange and $n = 5$ for the gluon exchange. Experimental data at 32 GeV/c (Table V) appear to favor slightly the quark exchange predictions.

The distributions of π^+'s in $\bar{p}p$ collisions become more and more symmetric with increasing topology. This may be explained by an increase of the annihilation, contributing mainly to multiprong topologies, and by the increase of the centrality of collisions. Minima in the distributions for the two-prong topology arise due to the asymmetry of $p/\bar{p}$ diffraction peaks because of not too good experimental resolution for leading particles. The figures demonstrate that $F_\pi^n(x)$ distributions become narrower both for pp and $\bar{p}p$ interactions with the increase of topology and their maxima become sharper. The solid line histograms shown in Figs. 11 and 12 correspond to the QGSM predictions, and one can note that the model reproduces the experimental $F_{\pi^\pm}(x)$ distributions reasonably well.

Figure 13 shows the double differential cross sections of π^+'s and π^-'s in pp interactions for four intervals of

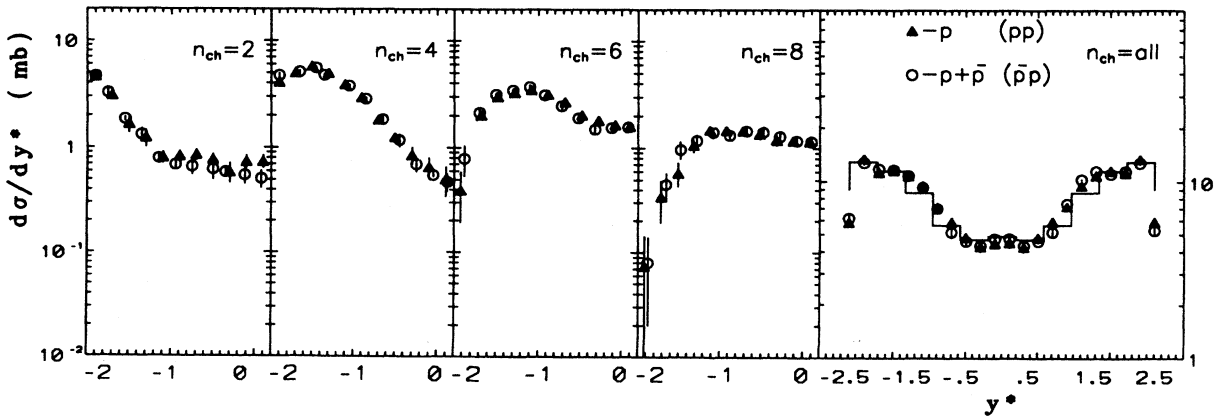

FIG. 8. Semi-inclusive and inclusive rapidity distributions of protons and antiprotons in pp and $\bar{p}p$ interactions at 32 GeV/c. Histogram denotes the QGSM predictions for protons in pp collisions.

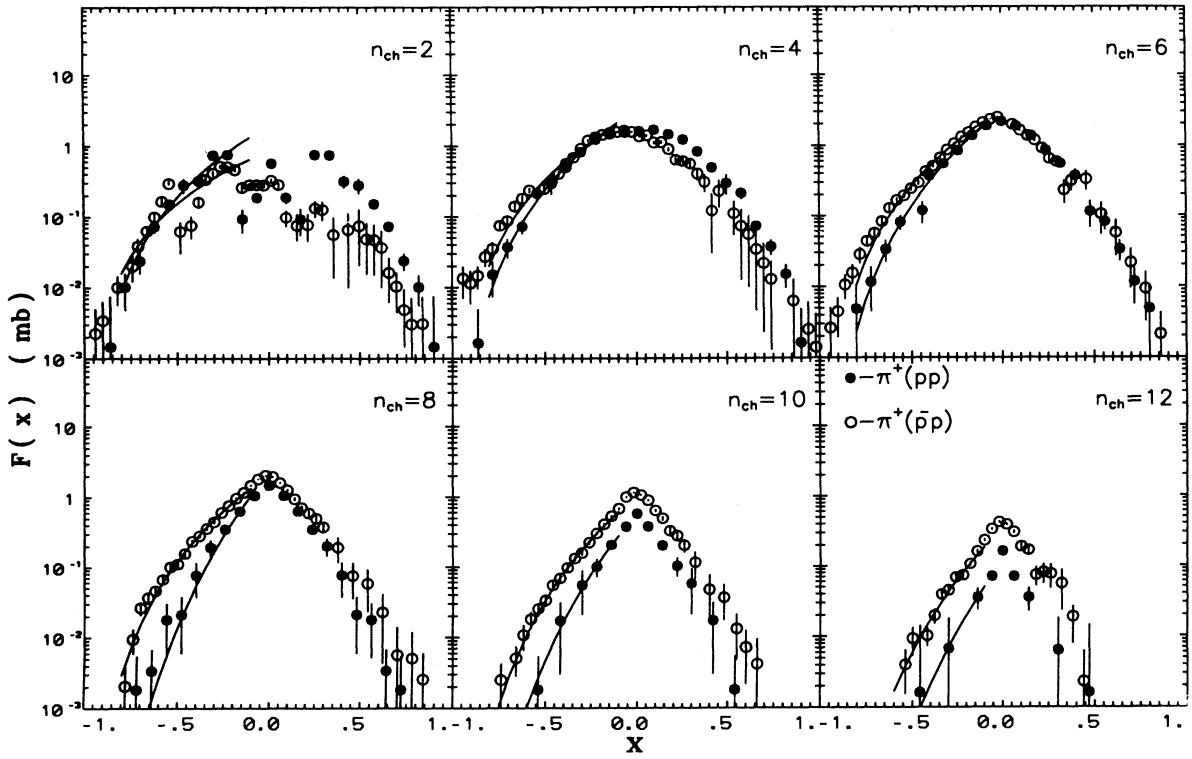

FIG. 10. Semi-inclusive invariant x distributions of π^+ mesons in pp and $\bar{p}p$ interactions at 32 GeV/c. The solid curves are the results of a fit to the power law $(1-|x|)^n$.

P_T^2. The slopes of the distributions are higher for the π^-'s. The normalized abundances of the yield of π^+'s in pp interactions,

$$\langle R_\pi \rangle = \frac{f_{\pi^+}(x,P_T^2) - f_{\pi^-}(x,P_T^2)}{f_{\pi^+}(x,P_T^2) + f_{\pi^-}(x,P_T^2)}, \tag{14}$$

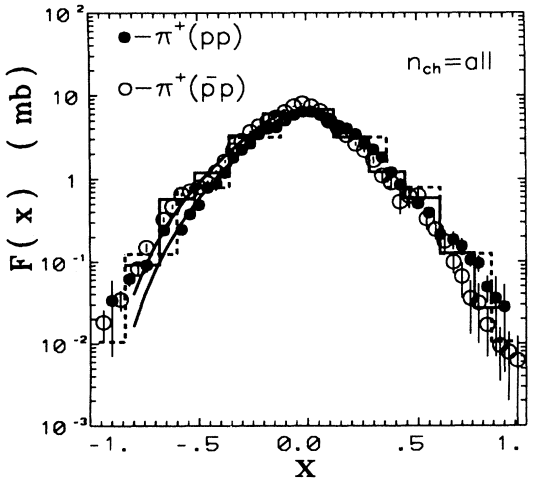

FIG. 11. Inclusive invariant x distributions of π^+ mesons in pp and $\bar{p}p$ interactions at 32 GeV/c. The solid curves are the results of a fit to the power law $(1-|x|)^n$ and the histograms are the predictions of the QGSM for π^+'s in $\bar{p}p$ (solid line) and pp (dashed line) interactions.

are shown as a function of x for the P_T^2 intervals and for all P_T^2 in Fig. 14. $\langle R_\pi \rangle$ seems to be slightly higher for the lowest P_T values. This behavior is opposite to that of $\langle R_\pi \rangle$ in $\bar{p}p$ interactions [3].

To compare the pion production in pp and $\bar{p}p$ interactions more clearly, in Fig. 15 we show the ratio

$$R_1 = \frac{F_{\pi^+}(pp) + F_{\pi^-}(pp)}{F_{\pi^+}(\bar{p}p) + F_{\pi^-}(\bar{p}p)} \tag{15}$$

TABLE V. The results of the fit of inclusive and semi-inclusive $F(x)$ distributions of π^+ mesons from pp and $\bar{p}p$ interactions at 32 GeV/c in the interval $-0.7 \le x \le -0.2$ to the power law $A*(1-|x|)^n$. Of each pair of numbers, the upper one is for pp and the lower one is for $\bar{p}p$ interactions.

Multiplicity	n	A (mb)	χ^2/N_{DF}
2 prong	3.38 ± 1.16	2.15± 0.17	14.29/5
inelastic	2.47 ± 0.12	0.84± 0.14	53.94/10
4 pr.	3.79 ± 0.19	3.64± 0.29	1.75/5
	2.82 ± 0.08	2.92± 0.13	28.56/10
6 pr.	4.39 ± 0.28	2.85± 0.32	1.97/5
	3.26 ± 0.07	3.33± 0.11	15.43/10
8 pr.	6.15 ± 0.72	4.30± 2.01	8.98/5
	3.94 ± 0.09	1.94± 0.08	7.18/10
10 pr.	7.44 ± 1.03	0.89± 0.23	0.98/3
	4.75 ± 0.19	0.94± 0.07	3.47/10
12 pr.	7.78 ± 3.38	0.12± 0.09	0.54/3
	5.83 ± 0.54	0.34± 0.07	4.69/6
All	3.98 ± 0.07	7.80± 0.29	19.82/10
	3.23 ± 0.06	8.76± 0.25	15.80/10

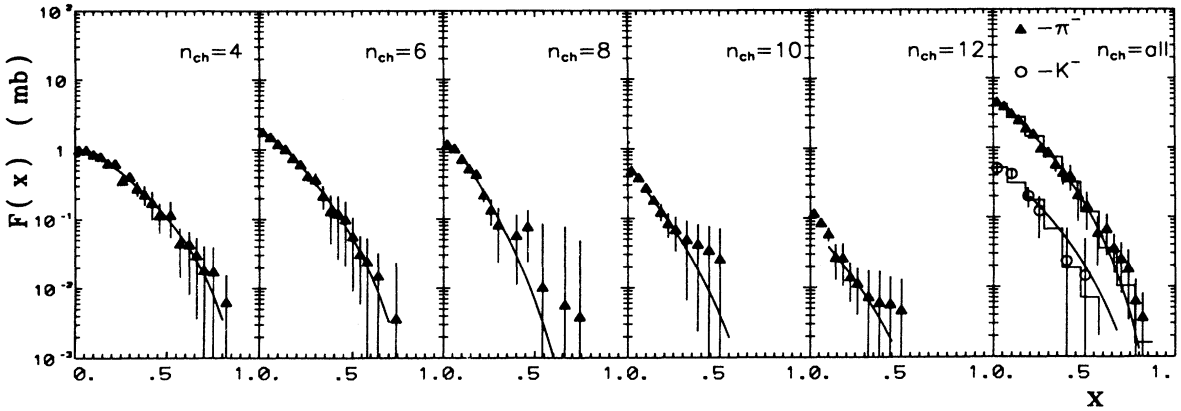

FIG. 12. Semi-inclusive and inclusive invariant x distributions of π^- and K^- mesons in pp interactions at 32 GeV/c. The solid curves are the results of a fit to the power law $(1-|x|)^n$ and solid-line histograms are the predictions of the QGSM.

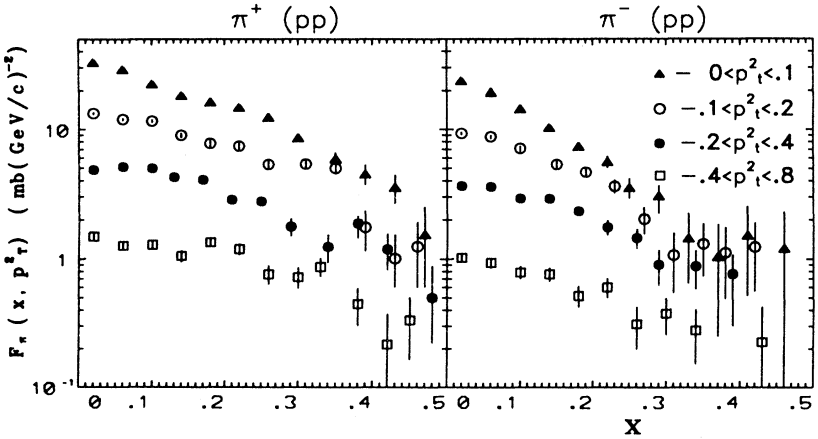

FIG. 13. Double differential invariant cross sections of π^+ and π^- mesons in pp interactions as a function of x for individual P_T^2 intervals.

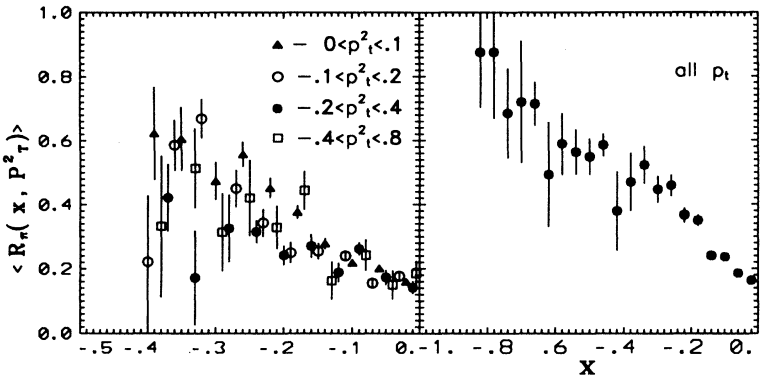

FIG. 14. The x distribution of $\langle R_\pi \rangle$ in pp interactions for individual P_T^2 intervals and for the whole P_T^2 region.

TABLE VI. The results of the fit of inclusive and semi-inclusive $F(x)$ distributions of π^- and K^- mesons from pp interactions at 32 GeV/c in the interval $0.2 \le x \le 0.7$ to the power law $A * (1-|x|)^n$. Of pair of numbers for total multiplicity, the upper one is for π^- and the lower one is for K^- mesons.

Multiplicity	n	A (mb)	χ^2/N_{DF}
4 pr.	4.45 ± 0.55	1.78± 0.32	5.91/8
6 pr.	5.50 ± 0.81	2.36± 0.60	0.98/8
8 pr.	4.69 ± 2.34	0.64± 0.45	1.41/5
10 pr.	3.83 ± 2.56	0.16± 0.14	0.26/4
All π^-	5.33 ± 0.75	5.62± 1.24	6.46/10
All K^-	4.90 ± 1.03	0.58± 0.07	1.38/4

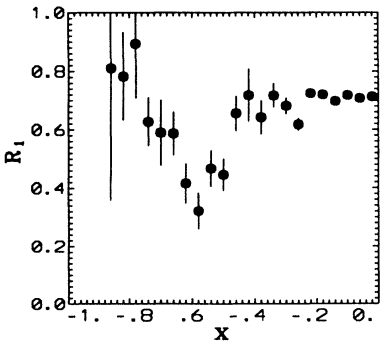

FIG. 15. The ratio of inclusive invariant x distribution of $\pi^\pm$'s in pp interactions to the same one in $\bar{p}p$ interactions.

in the backward hemisphere. This ratio is a constant in the central region, $R_1 \approx 0.72$ at $|x| < 0.45$, and it has a rather distinct minimum at $|x| = 0.6$. The origin of this minimum could be connected with the contamination of kaons, which are not separated from the spectrum of pions in $\bar{p}p$ collisions.

The investigation of the π^-'s rapidity distributions in pp and $\bar{p}p$ interactions can help to reveal some features of the $\bar{p}p$ annihilation. As seen in Sec. VI B above, the inclusive spectrum of protons in pp interactions practically coincides with the combined $p + \bar{p}$ spectrum in $\bar{p}p$ interactions at the energies in question, and so one may assume that

$$\frac{d\sigma_{\pi^-}}{dy^*}(pp) = \frac{d\sigma_{\pi^-}}{dy^*}(\bar{p}p_{\rm nonann}) \tag{16}$$

and the difference

$$\Delta_1 = \frac{d\sigma_{\pi^-}}{dy^*}(\bar{p}p) - \frac{d\sigma_{\pi^-}}{dy^*}(pp) \tag{17}$$

can be considered at $y < 0$ as an estimation of $\frac{d\sigma_{\pi^-}}{dy^*}(\bar{p}p)_{\rm ann}$. The rapidity distributions of π^-'s in both interactions, Δ_1, and the ratio

$$R_2 = \frac{d\sigma_{\pi^-}}{dy^*}(\bar{p}p_{\rm ann}) / \frac{d\sigma_{\pi^-}}{dy^*}(\bar{p}p_{\rm nonann}) \tag{18}$$

are shown in Fig. 16. The ratio R_2 increases with increasing y^* in the interval $-3 < y^* < -2$ and then falls. This behavior is similar to that at 12 GeV/c and at 100 GeV/c [27]. So the conclusion of [3] on a more narrow rapidity interval for pions from $\bar{p}p$ annihilation than from the nonannihilation process is not confirmed.

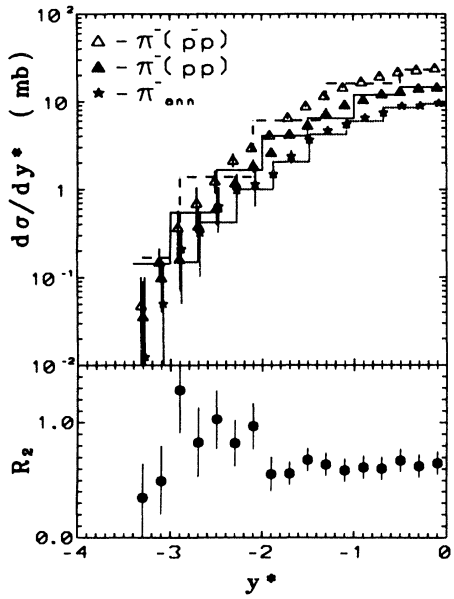

FIG. 16. c.m.s. rapidity distributions of π^- mesons in pp and $\bar{p}p$ interactions, their difference Δ_1, and ratio $R_2 = \frac{d\sigma_{\pi^-}}{dy}(\bar{p}p_{\rm ann}) / \frac{d\sigma_{\pi^-}}{dy}(\bar{p}p_{\rm nonann})$. Histograms denote the QGSM predictions.

TABLE VII. The results of the fit of inclusive and semi-inclusive $d\sigma/dy^*$ distributions of π^+ mesons from pp interactions at 32 GeV/c to formula (20).

Multiplicity	A (mb)	B	$\chi^2/N_{\rm DF}$
2 prong	5.54 ± 0.14	2.76± 0.18	87.20/26
4 pr.	23.69 ± 0.37	2.88± 0.11	139.55/19
6 pr.	21.51 ± 0.29	1.23± 0.02	56.85/17
8 pr.	11.47 ± 0.15	0.84± 0.02	28.36/15
10 pr.	4.25 ± 0.07	0.78± 0.03	17.79/22
12 pr.	0.96 ± 0.04	0.55± 0.05	8.28/16
All	65.41 ± 0.42	1.53± 0.18	93.29/18

In [3] the rapidity distributions of π^-'s in pp interactions were parametrized at 32 GeV/c according to the relation

$$\frac{d\sigma_{\pi^-}}{dy} = A \exp\left[-\frac{|y|}{D}\right]^B \tag{19}$$

proposed in [28] and values of the parameters A,B,D were found by the interpolation of the values obtained at neighboring energies in [27]. In the present paper the rapidity distributions of $\pi^\pm$'s are approximated by the Gaussian distribution

$$\frac{d\sigma}{dy^*} = A \exp\left[-\frac{y^{*2}}{2B}\right] \tag{20}$$

in accordance with the predictions of Landau's hydrodynamical model [29,30]. The c.m.s. inclusive and semi-inclusive rapidity distributions of π^+'s in $\bar{p}p$ and pp interactions are shown in Figs. 17, 18 together with the results of the fit to (20) (pp interactions only), which are also listed in Table VII. Inclusive and semi-inclusive rapidity distributions of π^-'s are shown in Fig. 19 and the results of their fits are given in Table VIII. The fitted curves are also projected onto the experimental data in Fig. 19. The histograms projected onto the inclusive distributions in Figs. 18 and 19 are the QGSM predictions. Landau theory in its original form established the Gaussian-like behavior for the pseudorapidity (Landau variable) distribution, but further solution of the full three-dimensional expansion problem proved that this is still valid for the rapidity distribution in the form [31,32]

$$\frac{dn}{dy} = \frac{\langle n \rangle}{\sqrt{2\pi L}} \exp\left(-\frac{y^2}{2L}\right), \tag{21}$$

where $\langle n \rangle$ means average multiplicity and

TABLE VIII. The results of the fit of inclusive and semi-inclusive $d\sigma/dy^*$ distributions of π^- and K^- mesons from pp interactions at 32 GeV/c to formula (20).

Multiplicity	A (mb)	B	$\chi^2/N_{\rm DF}$
4 pr.	10.10 ± 0.17	1.31± 0.03	78.44/16
6 pr.	14.75 ± 0.21	1.04± 0.03	24.87/15
8 pr.	9.20 ± 0.16	0.80± 0.03	22.91/14
10 pr.	3.59 ± 0.11	0.74± 0.04	8.91/14
All π^-	39.59 ± 0.27	1.08± 0.02	47.69/32
All K^-	2.03 ± 0.49	1.60± 0.51	0.25/7

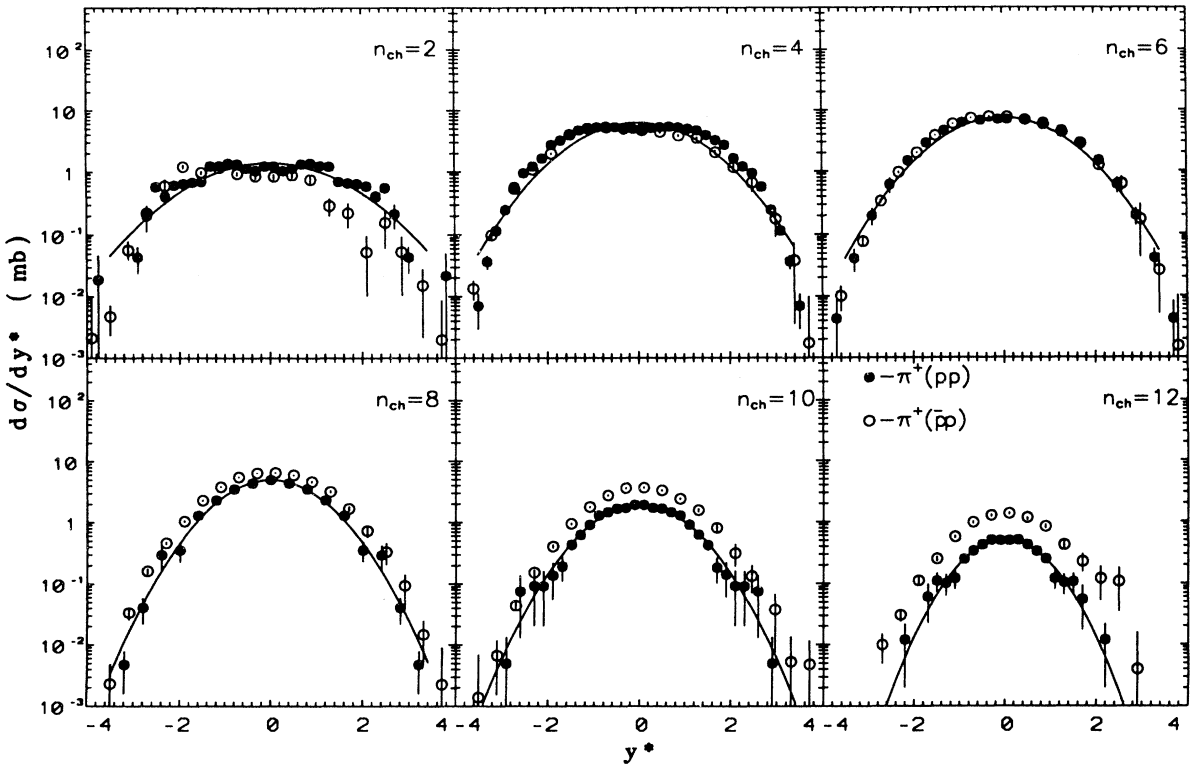

FIG. 17. Semi-inclusive rapidity distributions of π^+ mesons in pp and $\bar{p}p$ interactions at 32 GeV/c. The solid curves are the results of a Gaussian fit to (20) to π^+'s in pp interactions. The values of the fitting parameter B are listed in Table VII.

$$L = 0.5 \ln\left(\frac{E_{\rm lab}}{2m_p}\right) \tag{22}$$

or

$$L = \frac{2}{3}\left(\frac{1-c_0^2}{1-c_0^4}\right) \ln\left(\frac{E_{\rm lab}}{2m_p}\right). \tag{23}$$

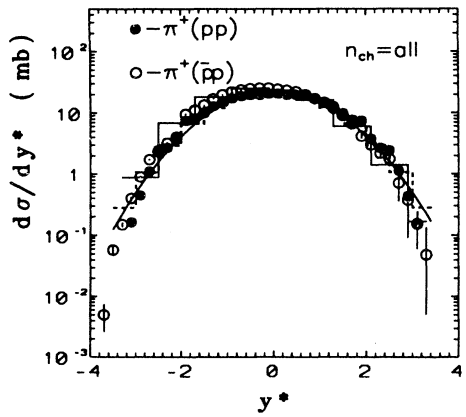

FIG. 18. Inclusive rapidity distributions of π^+ mesons in pp and $\bar{p}p$ interactions at 32 GeV/c. The solid curve denotes the result of a Gaussian fit to (20) to π^+'s in pp interactions. The value of the fitting parameter B is listed in Table VII. The histograms are the predictions of the QGSM for π^+'s in $\bar{p}p$ (solid line) and in pp (dashed line) interactions.

The parameter c_0^2 in the last expression means the squared velocity of sound. So in the case of an ultrarelativistic hadronic gas $c_0^2 = 1/3$ and both formulas predict the same result. If one takes into account the influence of resonances, the final value of c_0^2 will be $c_0^2 \approx 0.2$ [32]. Certainly, in order to test the applicability of the theory, one has to use the spectra of secondary particles from the nonfragmentation processes for fitting to (21). The comparison of the theoretical predictions to the results obtained for the y^* distributions of $\pi^{\pm}$'s and K^-'s in pp interactions at 32 and 69 GeV/c [12] shows (see Table IX) that the data appear to favor $c_0^2 = 1/3$. It should be mentioned that the model overestimates the width of the pion spectra, especially for π^-'s. For kaons, the hydrodynamic model slightly underestimates the experimental data, although the relatively big errors do not permit one to make a more definite conclusion. Therefore, it may be

TABLE IX. Comparison of the fit parameter B for the y^* distributions of π^-'s and K^-'s from pp interactions at 32 and 69 GeV/c with the predictions of hydrodynamic model.

	32 GeV/c	69 GeV/c
π^+	1.53± 0.18	1.79±0.13
π^-	1.08± 0.02	1.36±0.03
K^-	1.60± 0.51	-
$c_0^2 = 1/3$	1.436	1.809
$c_0^2 = 1/5$	1.595	2.010

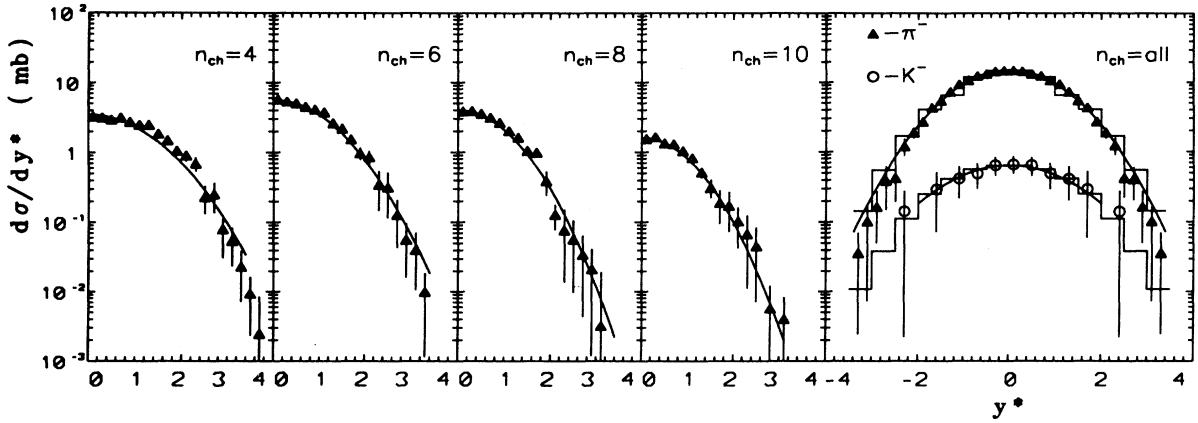

FIG. 19. c.m.s. rapidity distributions of π^- and K^- mesons in pp interactions at 32 GeV/c. The solid-line histograms are the predictions of QGSM and the solid curves are the results of a Gaussian fit to (20). The values of the fitting parameter B are listed in Table VIII.

more correct to compare the entire spectra of both neutral and charged mesons with the predictions of theory in Table IX.

The total spectrum of secondaries in both experiments can be approximated by a Gaussian distribution also. The total $1/\sigma_{\text{in}} d\sigma/dy^*$ distributions of secondary charged particles in the midrapidity region of pp and $\bar{p}p$ interactions are shown in Fig. 20, together with the results of a fit to (20). The parameters of the fit are

$$B_{\bar{p}p} = 4.46 \pm 0.02, \quad B_{pp} = 3.10 \pm 0.03 \ . \tag{24}$$

One interesting opportunity for searching for the quark-gluon plasma (QGP) in proton-antiproton annihilation is discussed in [33]. In accordance with one of the predictions of this paper, in the case of plasma creation quite noticeable fluctuations should take place in the central region of the dN/dy^* distribution. Figure 20 demonstrates that at 32 GeV/c these fluctuations are not observable

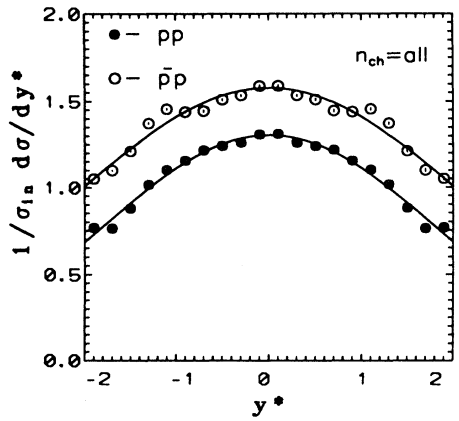

FIG. 20. $1/\sigma_{\text{in}}\ d\sigma/dy^*$ distribution of charged particles in pp and $\bar{p}p$ interactions at 32 GeV/c. The solid curves are the results of a Gaussian fit to (20). The values of the fitting parameter B are given in the text.

for the total charged particle spectrum or, at least, they should be smoothly distributed over the midrapidity region.

According to [34], particle distribution functions could demonstrate the limiting behavior in some region of phase space. Figure 21 shows the $d\sigma_{\pi^\pm}/dy^*$ distributions at 32 and 69 GeV/c [12] and their ratio

$$R_3 = \left(\frac{d\sigma_{\pi^\pm}}{dy^*}\right)_{32} \Big/ \left(\frac{d\sigma_{\pi^\pm}}{dy^*}\right)_{69} \ . \tag{25}$$

The structure functions $d\sigma/dy^*$ for positive and negative pions are still increasing in the midrapidity region with the growth of energy from 32 to 69 GeV/c. Such a behavior is quite different from that observed in $\bar{p}p$ interactions [3], where the $d\sigma/dy^*$ distributions of π^+ in the midrapidity region were found to be practically independent of energy, mainly due to the compensation of an increase of $(d\sigma_{\pi^+}/dy^*)_{y^*=0}$ in the nonannihilation processes by the decrease of $\bar{p}p$ annihilation.

In order to present relative magnitudes of $d\sigma_{\pi^\pm}/dy^*$ distributions, in Fig. 22 we show the ratio

$$R^{\pi}_{y^*} = \left(\frac{d\sigma_{\pi^+}}{dy^*} \Big/ \frac{d\sigma_{\pi^-}}{dy^*}\right)_{32,69} \tag{26}$$

and their differences

$$\Delta_2 = \frac{d\sigma_{\pi^+}}{dy^*} - \frac{d\sigma_{\pi^-}}{dy^*} \ . \tag{27}$$

(Results for 69 GeV/c are taken from [12].) It can be seen from these figures that at both energies the values of Δ_2 tend to increase with decreasing y^* in the midrapidity region and then decrease towards $y^* = 0$, while the ratios $R^{\pi}_{y^*}$ appear to decrease continually as $y^* \to 0$ and $R^{\pi}_{y^*}$ at 32 GeV/c lies slightly higher than $R^{\pi}_{y^*}$ at 69 GeV/c.

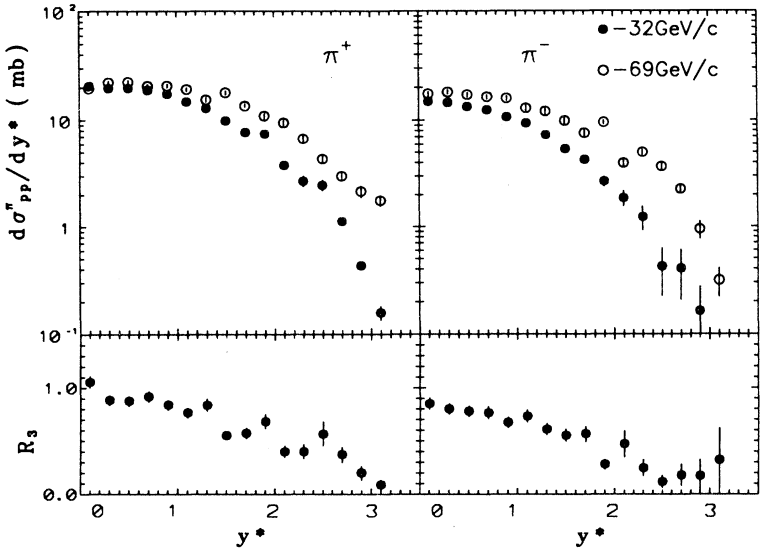

FIG. 21. Rapidity distributions of π^+ and π^- mesons in pp interactions at 32 and 69 GeV/c and their ratios R_3.

D. Inclusive distributions of negative kaons

The inclusive invariant distributions of negative kaons in pp interactions are presented in Fig. 12 [$F(x)$] and Fig. 19 ($d\sigma/dy^*$). The curve projected onto the $F_{K^-}(x)$ distribution shows the result of a fit to formula (13) in the interval $0.2 \leq x \leq 0.7$ with

$$n = 4.90 \pm 1.03 \ , \tag{28}$$

close to the value $n = 5$ predicted by the DCR. The results of the fit of the $d\sigma_{K^-}/dy^*$ distribution with (20) are listed in Table VIII and plotted in Fig. 19. The rapidity distribution of K^-'s is wider compared to those of $\pi^{\pm}$ in pp interactions. The QGSM predictions are shown in Figs. 12, 19 by solid line histograms. One can notice again that this model reproduces the shape of the inclusive distributions and particle cross sections reasonably well.

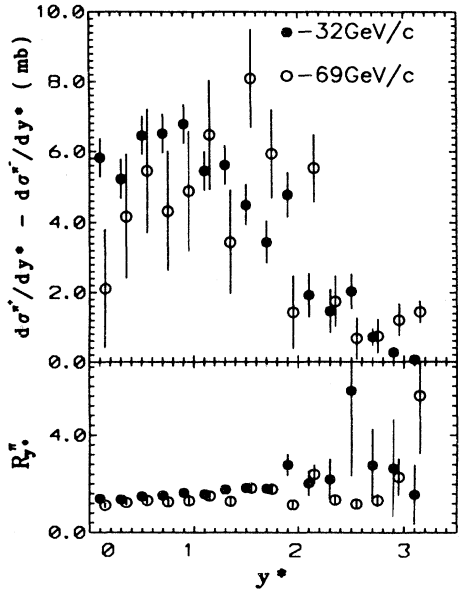

FIG. 22. The differences $\Delta_2 = d\sigma^{\pi^+}/dy^* - d\sigma^{\pi^-}/dy^*$ and the ratios $R^{\pi}_{y^*} = (\frac{d\sigma_{\pi^+}}{dy^*})/(\frac{d\sigma_{\pi^-}}{dy^*})$ for the reactions $pp \to \pi^{\pm} + X$ at 32 and 69 GeV/c.

VII. NONANNIHILATION $\bar{p}p$ AND pp INTERACTIONS

The annihilation process is among the most interesting processes in antiproton-proton collisions. It shows a number of differences from other hadronic low-P_T processes and, in particular, from the $\bar{p}p$ nonannihilation process [25]. It is, however, very difficult to determine whether these differences are due to kinematics (the presence of two baryons in the nonannihilation final state) or are related to dynamical differences between the annihilation and nonannihilation mechanisms. It is well known that the annihilation cross section decreases with the increase of energy as $\sim s^{-1/2}$. So almost all results on the inclusive characteristics of the $\bar{p}p$ annihilation process come from bubble chamber experiments at projectile momenta up to 12 GeV/c [14,25,35,36]. At higher energies (22.4, 32, 48.9, and 100 GeV/c) [37,3,38,13], differences of pion inclusive distributions in pp and $\bar{p}p$ experiments have been investigated.

In order to study annihilation at high energies one has to apply one of the possible methods mentioned in [25].

(A) Kinematic fitting to exclusive channels. Using this technique, the rapidity distributions for π^+ mesons in $\bar{p}p$ annihilation at 32 GeV/c were investigated in [39].

(B) Direct identification of baryons and antibaryons in nonannihilation. In bare bubble chamber experiments the identification is possible only for a restricted phase space region because one can separate, for instance, proton and pion tracks by ionization only for $P_{\rm lab} \leq 1.2$ GeV/c. This means that no more than about half of the

TABLE X. Numbers of events with identified protons and their topological cross sections in pp and $\bar{p}p$ interactions.

Multiplicity	$N_{\mathrm{Pid}}(pp)$	$N_{\mathrm{Pid}}(\bar{p}p)$	$\sigma_{\mathrm{Pid}}^{pp}$ (mb)	$\sigma_{\mathrm{Pid}}^{\bar{p}p}$ (mb)
2 pr.	5611	15877	3.12 ±0.10	2.77±0.06
4 pr.	7359	24443	4.79 ±0.10	4.70±0.05
6 pr.	2941	13095	2.23 ±0.05	2.24±0.03
8 pr.	761	3248	0.66 ±0.05	0.60±0.02
10 pr.	120	537	0.12 ±0.01	0.12±0.01
All	16803	57277	10.91 ±0.14	10.45±0.08

protons can be identified at our energies.

(C) Kinematic cuts for baryon production. For example, events of the type $\bar{p}p \rightarrow \bar{n}n+$ pions will have a larger missing mass than $\bar{p}p \rightarrow$ pions.

(D) Subtraction of $\bar{p}p$ and pp data. This method is based on the assumption that the differences between $\bar{p}p$ and pp interactions are caused by the $\bar{p}p$ annihilation process. Detailed investigation of this problem at 8.8 and at 32 GeV/c [25,39] seems to reveal some restrictions concerning the validity of the method, although this question is not quite clear even now.

The most reliable results come from events with directly identified baryons and antibaryons in the final state. For extracting the results presented, technique (B) was used. Following [40], the proton and $\pi^{\pm}$ $d\sigma/dx$ and $d\sigma/dP_T^2$ distributions were compared, for the events with slow protons ($P_{\mathrm{lab}} \leq 1.2$ GeV/c which corresponds to $x \leq -0.3$) identified by ionization. In this case the kinematic conditions should be the same for pp and $\bar{p}p$ interactions. In Table X the numbers of events with identified protons are listed for the different multiplicities together with the corresponding topological cross sections, both for pp and for $\bar{p}p$ collisions. Except for two-prong events, all topological cross sections practically coincide for pp and $\bar{p}p$ interactions.

Other secondaries in these events are assumed to be pions. In Figs. 23 and 24 the differential cross sections $d\sigma/dx$ are presented for identified protons and "pions," and Figs. 25 and 26 show $d\sigma/dP_T^2$ distributions for the same particles. The forward-backward asymmetry of $d\sigma/dx$ distributions, especially significant for the two- to six-prong topologies, arises due to proton (antiproton) contamination due to lack of identification for $P_{\mathrm{lab}} > 1.2$ GeV/c. P_T^2 distributions for protons are fitted by the formula

$$\frac{d\sigma}{dP_T^2} = A\exp(-BP_T^2) \ . \tag{29}$$

The values of the slope parameter B are listed in Table XI. The first fact that can be mentioned from Figs. 23, 24, and from Table XI, is the similarity of the spectra of identified protons in pp collisions and in $\bar{p}p$ collisions within the errors. This means that there are no significant differences in the behavior of slow protons in pp and $\bar{p}p$ interactions at 32 GeV/c. This conclusion contradicts the results of [40] where distinct differences in the shapes of identified proton and positive pion spectra were found for nonannihilation $\bar{p}p$ and pp collisions by the comparison of $\bar{p}p$ interactions at 22.4 GeV/c to pp interactions at nearby energies.

Unfortunately, it is very difficult to compare our results with the data from [25] at 8.8 GeV/c. There the total samples of pp and $\bar{p}p$ nonannihilation collisions were investigated and the comparison was done for the total π^+, π^-, and π^c spectra. A comparison of the production cross sections and invariant distributions of neutral strange particles in pp and nonannihilation $\bar{p}p$ interactions at 32 GeV/c was done in [41]. The results obtained in this paper demonstrate the similarity of strange particle spectra in both interactions within a few percent of accuracy.

The main conclusions of this section can be drawn as follows.

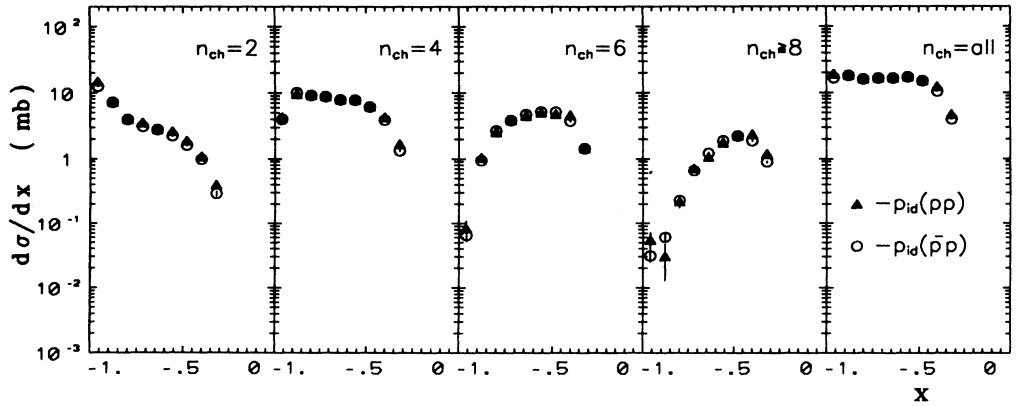

FIG. 23. Semi-inclusive and inclusive $d\sigma/dx$ distributions of protons identified by ionization in pp and $\bar{p}p$ interactions at 32 GeV/c.

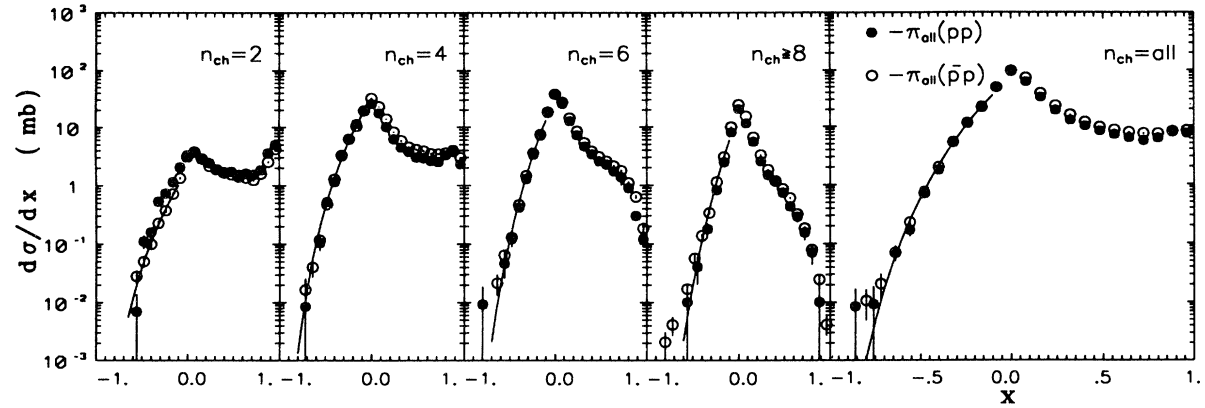

FIG. 24. Semi-inclusive and inclusive $d\sigma/dx$ distributions of charged particles assumed to be pions in the reactions $pp(\bar{p}p) \to p_{id} + X$ at 32 GeV/c. The solid curves are the results of a fit to the power law $(1 - |x|)^n$.

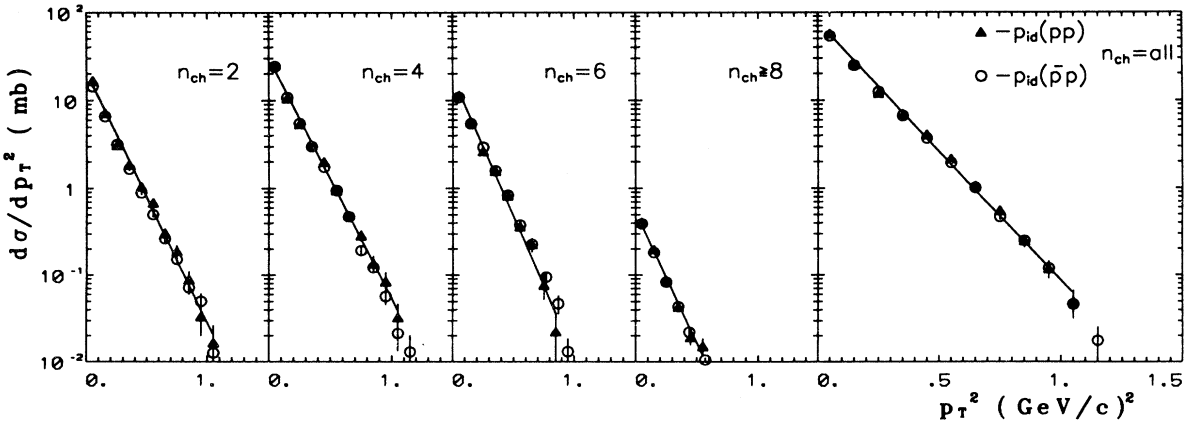

FIG. 25. Semi-inclusive and inclusive P_T^2 distributions of protons identified by ionization in pp and $\bar{p}p$ interactions at 32 GeV/c. The solid lines are the results of a fit to formula (29).

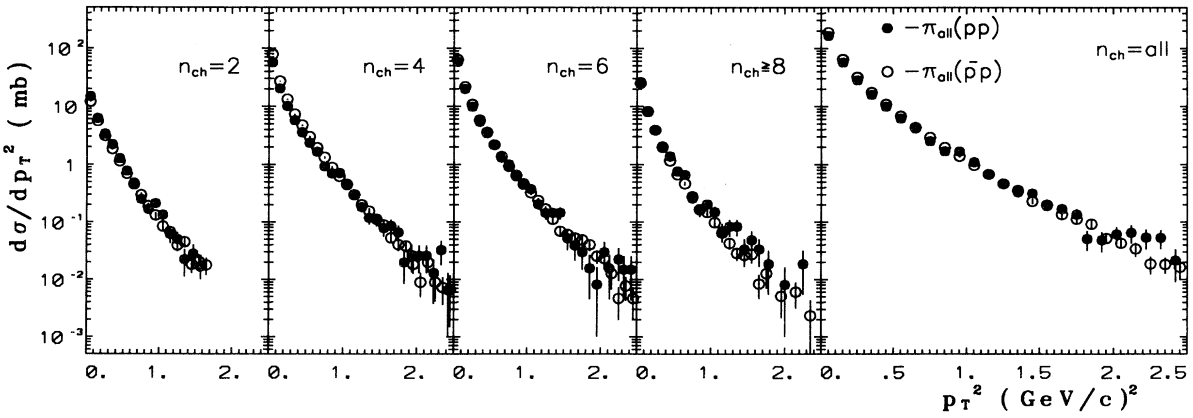

FIG. 26. Semi-inclusive and inclusive P_T^2 distributions of charged particles assumed to be pions in the reactions $pp(\bar{p}p) \to p_{id} + X$ at 32 GeV/c.

TABLE XI. The results of the fit of P_T^2 distributions of identified protons to the expression $A\exp(-BP_T^2)$.

Multiplicity	A [mb/(GeV/c)^2]	B [(GeV/c)$^{-2}$]	χ^2/N_{DF}
2 prong	22.39 ± 0.48	7.11± 0.12	8.54/11
4 pr.	32.45 ± 0.60	6.70± 0.09	8.56/11
6 pr.	15.47 ± 0.41	6.82± 0.13	1.34/9
≥ 8 pr.	0.59 ± 0.03	7.48± 0.27	0.34/6
All	75.91 ± 0.91	6.86± 0.06	12.01/11

There are no differences between the spectra of identified protons ($P_{\rm lab} \leq 1.2$ GeV/c) in pp and $\bar{p}p$ interactions at 32 GeV/c.

The topological cross sections of the processes with an identified proton are practically the same.

Total $d\sigma/dx$ spectra of other charged particles, presumed to be pions, demonstrate also a similar behavior within the data accuracy with one possible exception for the two-prong topology (Fig. 24).

VIII. TRANSVERSE MOMENTUM DISTRIBUTIONS AND AVERAGE VALUES

Transverse momentum distributions play a significant role in the investigation of the dynamics of particle-particle collisions. These data, especially inclusive yields of secondaries with intermediate ($1 < P_T < 3$ GeV/c) and large P_T, are very important for the comparison to predictions of various models of soft hadron-hadron interactions. They help to reveal the role of different subprocesses between the constituents in the collisions.

To obtain average P_T values, the following set of definitions is used:

$$\langle P_T \rangle = \int P_T \frac{d^2\sigma}{dx\, dP_T^2} dP_T^2 \Big/ \int \frac{d^2\sigma}{dx\, dP_T^2} dP_T^2 , \quad (30)$$

$$\langle P_T^2 \rangle = \int P_T^2 \frac{d^2\sigma}{dx\, dP_T^2} dP_T^2 \Big/ \int \frac{d^2\sigma}{dx\, dP_T^2} dP_T^2 , \quad (31)$$

and

$$\langle P_T \rangle_E = \int E^* P_T \frac{d^2\sigma}{dx\, dP_T^2} dP_T^2 \Big/ \int E^* \frac{d^2\sigma}{dx\, dP_T^2} dP_T^2 . \quad (32)$$

An investigation of $\langle P_T \rangle_E$ and P_T^2 distributions, including their comparison with the predictions from the quark fusion model (QFM) [42] and the constituent interchange model (CIM) [43] was performed on a part of the statistics (≈ 55 000 events) for $\bar{p}p$ interactions at 32 GeV/c in [3]. A detailed study of inclusive and semi-inclusive transverse momentum distributions of charged hadrons in $\bar{p}p$ interactions (≈ 165 000 inelastic events) is published in [44]. So the results of this section will be mainly devoted to transverse momentum distributions of charged secondaries in pp interactions at 32 GeV/c, to their comparison to the $\bar{p}p$ data at the same energy, and to the investigation of contributions from different diagrams in the framework of the QGSM.

A. P_T^2 distributions

For the approximation of $d\sigma/dP_T^2$ distributions in the entire P_T^2 region we used the standard phenomenological fit to the sum of two exponents,

$$\frac{d\sigma}{dP_T^2} = A\exp(-\alpha P_T^2) + B\exp(-\beta P_T^2) , \quad (33)$$

and by the power-law dependence

$$\frac{d\sigma}{dP_T^2} = \frac{A}{(1 + B\, P_T^2)^n} . \quad (34)$$

Usually, the first form is explained by the existence of directly produced hadrons, characterized by a universal slope parameter $\alpha \approx 3.5$, and hadron production from resonance decays which contribute to a low-P_T part of the P_T^2 distribution. Another possible approximation of the transverse momentum distributions is suggested by the experimental fact that the spectra of secondaries are better described by an exponential m_T dependence than a P_T one [45,46]:

$$\frac{d\sigma}{dP_T^2} = A\, \frac{m_T}{T}\, K_1\Big(\frac{m_T}{T}\Big) , \quad (35)$$

where $m_T = \sqrt{P_T^2 + m^2}$ is a transverse mass and K_1 is the modified Bessel function. A number of statistical models of multiparticle production invoke the hypothesis of local thermal equilibrium and link the slope T to a temperature of a thermalized system.

The inclusive and semi-inclusive P_T^2 distributions of charged particles in pp and $\bar{p}p$ interactions at 32 GeV/c are shown in Figs. 27–29. The results of the fits of these distributions to formulas (33)–(35) are listed in Tables XII–XIV. They are plotted also on the P_T^2 distributions of protons in Fig. 27 [fits to the formulas (33) and (35)], and on the same distributions of $\pi^{\pm}$'s and K^-'s in Figs. 28, 29, where the results of the fit to formula (35) are shown. It is easy to see that the approximation by the sum of two exponents (33) provides the best description of the experimental spectra in the region $P_T^2 \leq 2$ (GeV/c)^2 among the expressions (33)–(35), but it does not reproduce the long tails of the transverse momentum distributions (Fig. 27). The fit with the function (34) gives the worst results, and the transverse mass dependence (35) provides the best overall approximation of the shape of charged particle P_T^2 distributions, although it contains only two fit parameters. The value of the slope parameter T is close to the predicted value $T \approx m_\pi$ for charged mesons, while it is much smaller for the proton spectra.

B. Average values of P_T

Bubble chamber experiments permit one to measure all tracks of charged particles including the low-P_T ones. This circumstance is very important for the true determination of average P_T values. The region of small P_T contributes dominantly to $\langle P_T \rangle$ and many other experiments

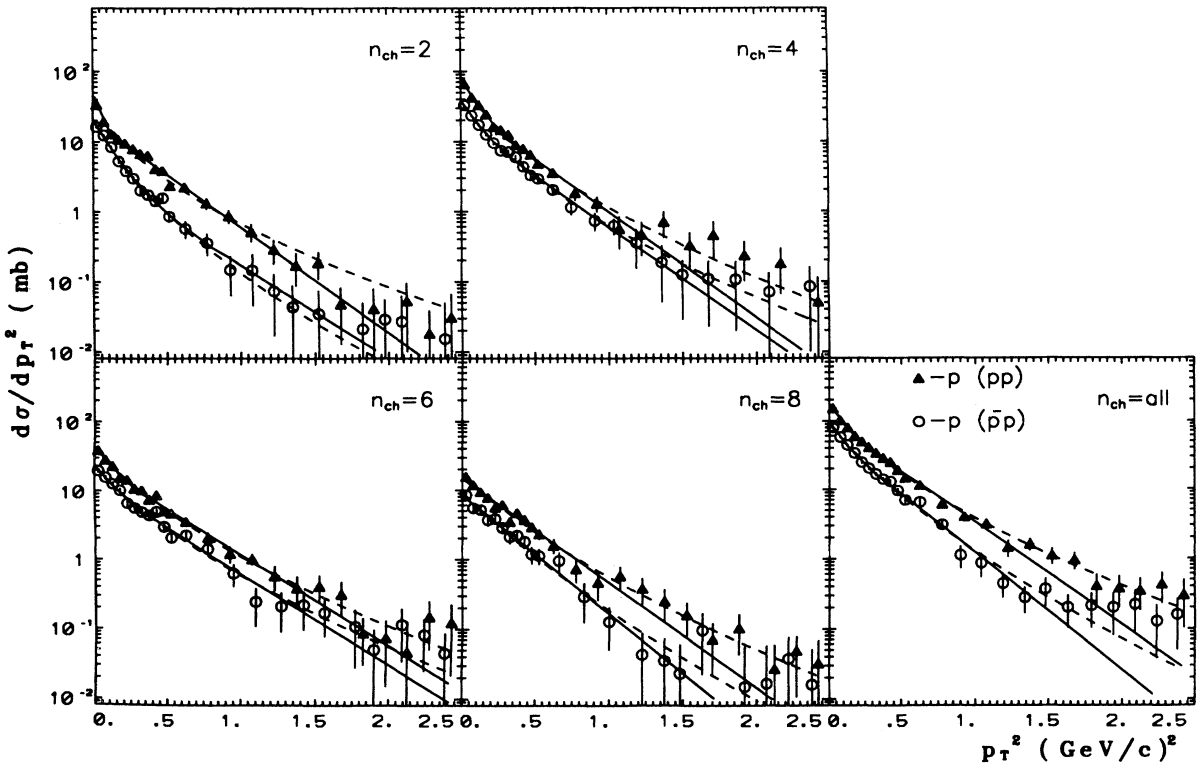

FIG. 27. Semi-inclusive and inclusive P_T^2 distributions of protons and antiprotons in pp and $\bar{p}p$ interactions at 32 GeV/c. The solid curves represent the results of a fit to the expression (33); the dashed curves correspond to the results of a fit to formula (35).

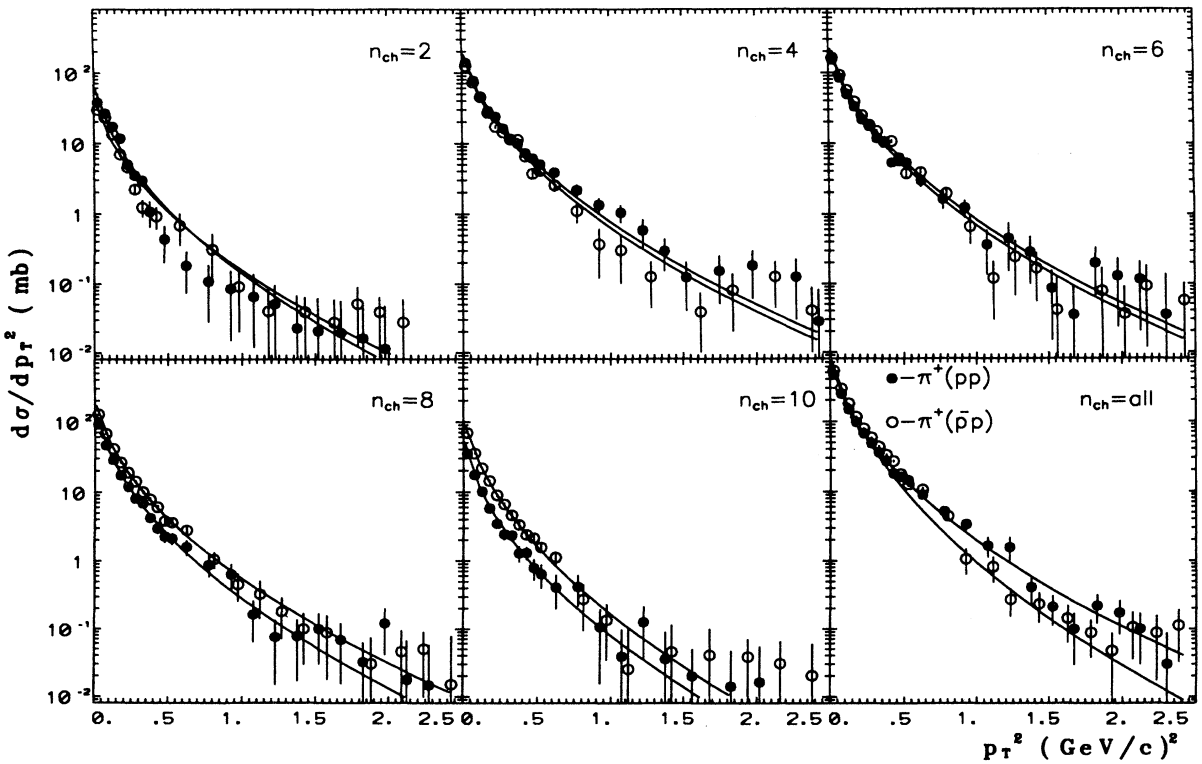

FIG. 28. Semi-inclusive and inclusive P_T^2 distributions of π^+'s in pp and $\bar{p}p$ interactions at 32 GeV/c. The solid curves represent the results of a fit to formula (35).

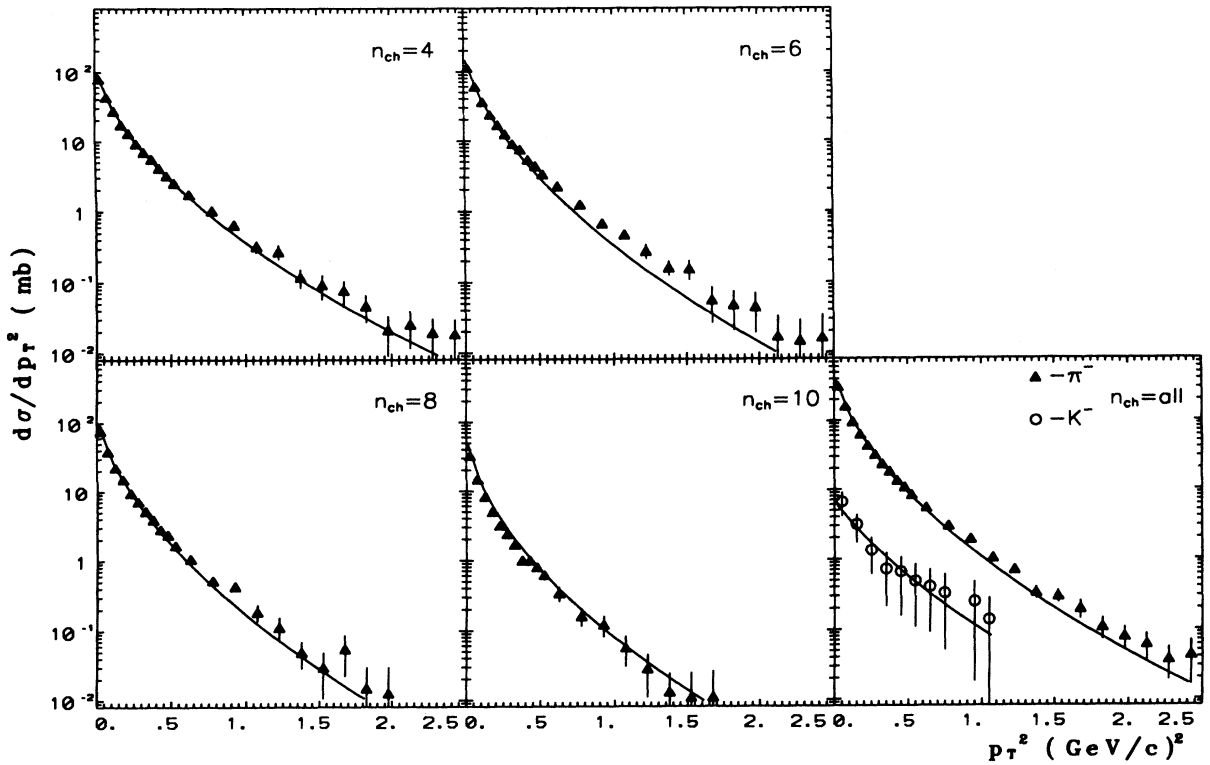

FIG. 29. The P_T^2 distributions of π^-'s (inclusive and semi-inclusive) and K^-'s (inclusive) in pp and $\bar{p}p$ interactions at 32 GeV/c. The solid curves represent the results of a fit to formula (35).

have cuts below, say, 0.15–0.4 GeV/c. The average values of P_T, P_T^2, and the dispersion $D = (\langle P_T^2\rangle - \langle P_T\rangle^2)^{1/2}$ are listed in Table XV for inclusive particle production in pp and $\bar{p}p$ interactions. The claim of all statistical models is that the transverse momentum distribution below $P_T \approx 1$ GeV/c is thermal. Different approaches are possible for the description of the transverse momentum distribution:

$$\langle P_T\rangle = \left(\frac{\pi m T}{2}\right)^{1/2} \frac{K_{5/2}(m/T)}{K_2(m/T)} \tag{36}$$

[statistical bootstrap model (SBM) [45,47], particles obey Boltzmann statistics],

$$\langle P_T\rangle = \left(\frac{\pi m T}{2}\right)^{1/2} \frac{K_2(m/T)}{K_{3/2}(m/T)} \tag{37}$$

[SBM, $d\sigma/dP_T^2 \propto \exp(-m_T/T)$], or

$$\langle P_T\rangle \approx 2.12 T_0 \tag{38}$$

(hydrodynamic model, if the transverse velocity initially vanishes [48]).

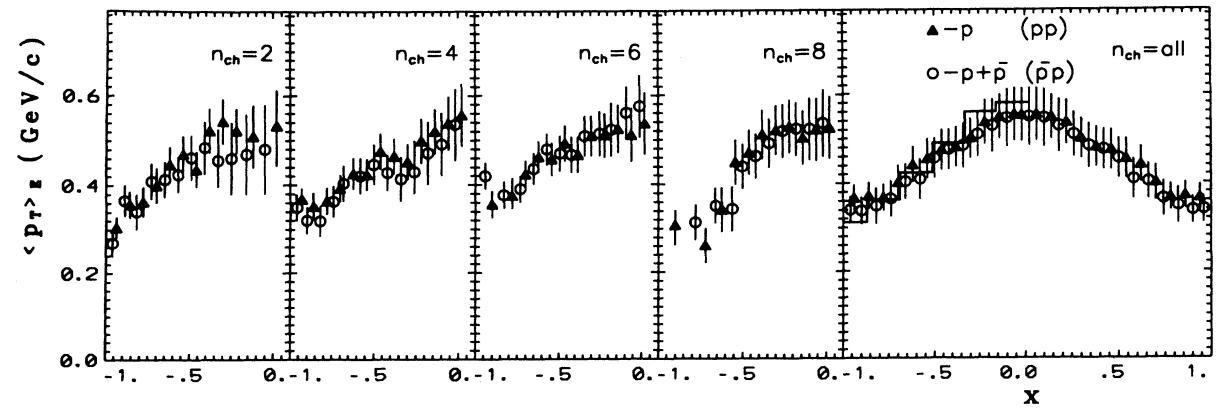

FIG. 30. The x dependence of $\langle P_T\rangle_E$ for protons and protons plus antiprotons in pp and $\bar{p}p$ interactions at 32 GeV/c. The histogram denotes the QGSM predictions for protons in pp collisions.

The predictions of these models for $\pi^{\pm}$ mesons in pp and $\bar{p}p$ interactions at 32 GeV/c are listed in Table XVI. As can be seen from this table the models either overestimate or underestimate the values of $\langle P_T \rangle$ for pions at $T_0 = T_\pi \approx m_\pi$. In hydrodynamics this fact can be explained by the influence of the collective transverse flow, which has recently been the focus of many investigations.

The comparison of multiparticle production in pp and $\bar{p}p$ interactions is continued in terms of the correlation of the transverse and longitudinal momenta of secondaries. Figure 30 shows the $\langle P_T \rangle_E$ as a function of x for inclusive and semi-inclusive production of protons (pp) and $p + \bar{p}$ ($\bar{p}p$), Fig. 31 shows the same distributions for π^+'s in both experiments, and Fig. 32 presents $\langle P_T \rangle_E$ as a function of x for π^- in pp interactions. The distributions of negative and positive pions have an evident minimum in the central region (the so-called "seagull" effect), which becomes more distinct with increasing $n_{\rm ch}$, while the opposite effect appears to be true for the proton and combined spectra. The distribution of negative particles assumed to be pions in pp interactions is presented in Fig. 32. It demonstrates that kaon contamination is negligibly small compared to π^-'s in the central region of the $\langle P_T \rangle_E$ distribution of negative particles.

To elaborate on the role of different subprocesses in the seagull-like shape of the average momentum distribution, $\langle P_T^2 \rangle$ is shown in Fig. 33 as a function of x for the diagrams invoked in the QGSM for the description of $\bar{p}p$ interactions. It can be seen from the figure that the seagull effect for pions is mainly due to multichain processes [Fig. 2(b)] including the annihilation process [Figs. 2(g), 2(h), 2(i)]. The seagull-like shape for pions depends on the transverse momentum of the leading particles, because $\langle P_T \rangle$ of particles from the central x region is always small in the QGSM. These leading pions are produced at the ends of the heavy diquark strings with

TABLE XII. The results of the fit of inclusive and semi-inclusive $d\sigma/dP_T^2$ distributions of charged particles from pp and $\bar{p}p$ interactions at 32 GeV/c in the interval $0 < P_T^2 < 2$ (GeV/c)^2 to expression (33).

Multiplicity	A [mb/(GeV/c)^2]	α [(GeV/c)$^{-2}$]	B [mb/(GeV/c)^2]	β [(GeV/c)$^{-2}$]	$\chi^2/N_{\rm DF}$
$pp \to p + X$					
2 pr.	32.99 ± 4.09	30.81 ± 4.97	20.10 ± 0.96	3.51 ± 0.13	22.37/17
4 pr.	48.06 ± 4.72	11.66 ± 1.67	31.67 ± 5.34	3.47 ± 0.28	24.89/18
6 pr.	22.03 ± 3.07	11.37 ± 2.59	23.41 ± 2.89	3.01 ± 0.18	20.52/18
8 pr.	9.78 ± 3.58	7.58 ± 2.99	16.60 ± 3.37	3.21 ± 0.18	21.04/16
10 pr.	5.11 ± 0.55	4.14 ± 0.41	6.8E-3± 0.13	-0.89 ± 1.09	7.66/16
All	86.68 ± 6.70	15.13 ± 2.55	99.06 ± 7.12	3.41 ± 0.14	44.10/18
$\bar{p}p \to \bar{p} + X$					
2 pr.	16.89 ± 1.22	8.86 ± 0.81	3.53 ± 1.29	3.03 ± 0.44	18.71/17
4 pr.	22.43 ± 3.08	11.35 ± 2.32	17.50 ± 3.42	3.40 ± 0.32	11.79/17
6 pr.	10.92 ± 2.71	9.31 ± 2.69	12.21 ± 2.60	3.02 ± 0.29	24.11/17
8 pr.	11.45 ± 4.20	3.69 ± 0.67	-3.18 ± 4.46	3.27 ± 1.17	7.31/16
10 pr.	2.87 ± 0.79	5.13 ± 1.33	0.28 ± 0.46	1.77 ± 0.95	9.57/16
All	42.48 ± 6.52	8.42 ± 0.73	45.81 ± 5.67	3.56 ± 0.16	30.16/18
$pp \to \pi^+ + X$					
2 pr.	49.34 ± 1.26	9.07 ± 0.24	0.08 ± 0.13	0.82 ± 0.97	25.55/15
4 pr.	156.30 ± 4.10	14.87 ± 0.72	34.17 ± 3.92	3.53 ± 0.22	19.87/17
6 pr.	165.67 ± 5.17	14.98 ± 0.79	41.05 ± 5.64	4.11 ± 0.28	23.02/18
8 pr.	104.70 ± 4.58	16.77 ± 1.36	25.98 ± 5.43	4.70 ± 0.46	20.18/18
10 pr.	42.78 ± 2.23	15.73 ± 1.40	6.28 ± 1.99	4.15 ± 0.61	6.75/16
All	508.14 ± 9.24	15.05 ± 0.48	119.16 ± 9.98	4.12 ± 0.17	27.18/18
$\bar{p}p \to \pi^+ + X$					
2 pr.	37.50 ± 0.37	9.20 ± 0.21	0.06 ± 0.05	0.28 ± 0.52	59.42/13
4 pr.	127.32 ± 4.97	15.19 ± 0.83	43.07 ± 5.17	4.55 ± 0.26	51.79/15
6 pr.	156.78 ± 5.63	15.73 ± 0.82	62.03 ± 6.22	4.81 ± 0.22	49.74/16
8 pr.	133.44 ± 4.62	17.32 ± 1.08	45.97 ± 5.42	4.79 ± 0.28	14.52/16
10 pr.	67.80 ± 4.05	19.30 ± 2.09	31.02 ± 4.94	5.80 ± 0.41	12.43/15
All	511.90 ±11.49	16.59 ± 0.55	215.44 ±12.94	5.13 ± 0.14	35.30/17
$pp \to \pi^- + X$					
4 pr.	84.42 ± 1.81	14.42 ± 0.56	21.49 ± 1.79	3.90 ± 0.15	38.21/18
6 pr.	125.02 ± 2.36	15.73 ± 0.54	31.58 ± 2.23	4.14 ± 0.14	31.09/18
8 pr.	86.25 ± 2.25	17.14 ± 0.82	22.49 ± 2.24	4.74 ± 0.21	26.77/17
10 pr.	40.79 ± 1.53	18.11 ± 1.11	6.87 ± 1.06	4.65 ± 0.32	10.71/15
All	353.55 ± 3.84	15.61 ± 0.31	76.79 ± 3.42	4.06 ± 0.09	39.89/20
$pp \to K^- + X$					
All	9.93 ± 5.98	11.41 ± 7.52	1.32 ± 1.79	1.98 ± 1.73	0.26/6

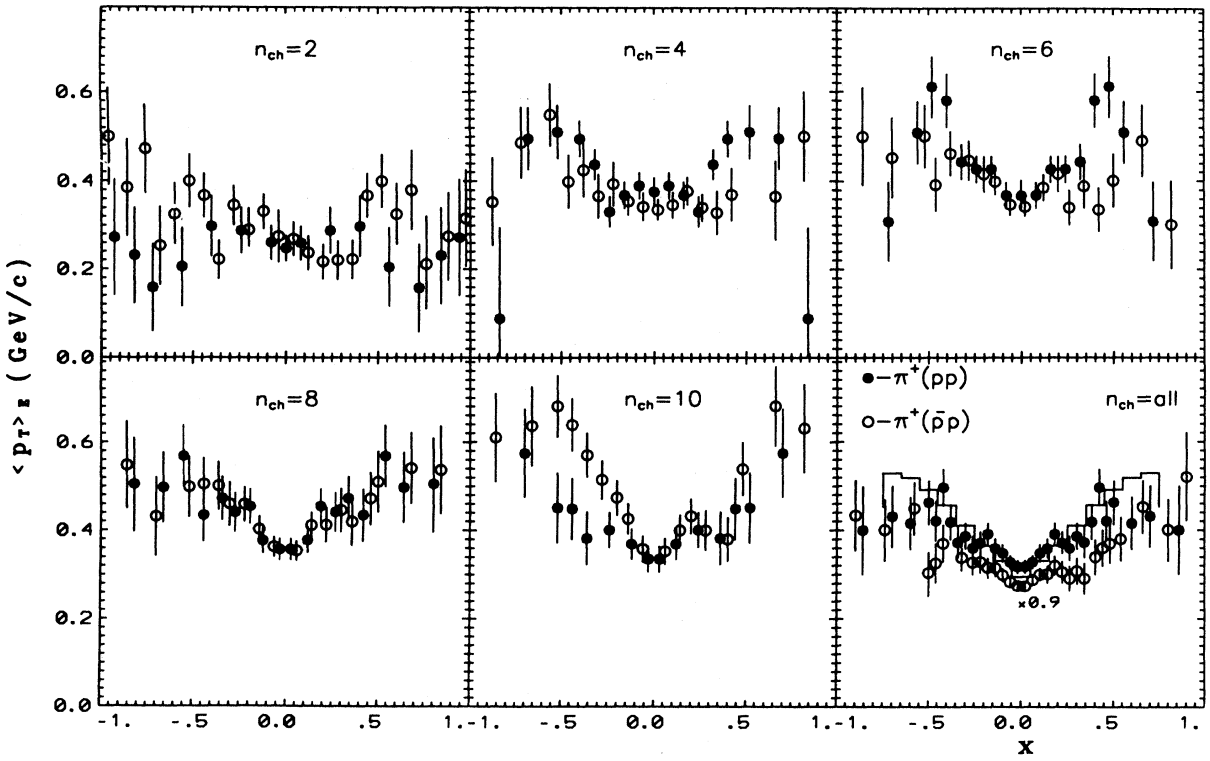

FIG. 31. The x dependence of $\langle P_T \rangle_E$ for π^+'s in pp and $\bar{p}p$ interactions at 32 GeV/c. The inclusive spectrum of $\pi^+(\bar{p}p)$ is multiplied by factor of 0.9. The histogram denotes the QGSM predictions for π^+'s in pp-collisions.

initial large $\langle P_T \rangle$ in multichain or annihilation processes. Therefore, their average transverse momentum should be higher than those from the central region.

IX. CONCLUSIONS

Our investigation of various inclusive and semi-inclusive distributions of charged particles in pp and $\bar{p}p$ interactions at 32 GeV/c permits the following conclusions to be drawn.

(1) The total inclusive production cross sections of charged particles are measured in both interactions.

(2) The longitudinal and transverse momentum distributions of charged particles are measured in both interactions.

(3) The semi-inclusive cross sections of proton produc-

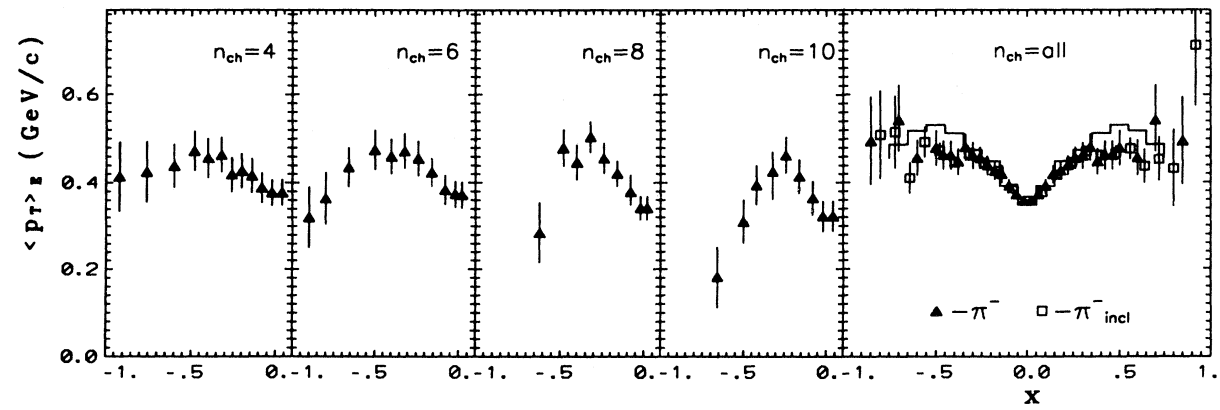

FIG. 32. The x dependence of $\langle P_T \rangle_E$ for π^-'s and for negatively charged particles assumed to be pions in pp interactions at 32 GeV/c. The histogram denotes the QGSM predictions for π^-'s in pp collisions.

tion are found to be equal in both interactions.

(4) The inclusive spectra of protons in pp interactions coincide within the accuracy of the data with the combined proton plus antiproton spectra in $\bar{p}p$ interactions. It means that the contribution of the planar diagram [Fig. 2(a)] in $\bar{p}p$ interactions at 32 GeV/c is small.

(5) Nonannihilation $\bar{p}p$ interactions and pp interactions appear to be similar within the errors. This behavior is different from the one observed at lower energies.

(6) The height of the rapidity distribution of protons at $y^* = 0$ is $(d\sigma/dy^*)_{y^*=0} = 4.6 \pm 0.2$ mb and does not depend on the projectile momentum from 24 to 69 GeV/c.

(7) The rapidity distributions of charged mesons in pp interactions are well approximated by a Gaussian fit. The same form of particle rapidity distribution is predicted by the Landau hydrodynamic model, but extracting parameters compatible with theory predictions is a delicate problem which deserves further investigations.

(8) Also the total rapidity distributions of secondary charged particles are well described by the Gaussian expression, both in pp and in $\bar{p}p$ interactions. There are no noticeable deviations in the $1/\sigma_{\text{in}} \sum d\sigma_i/dy^*$ distribution of secondaries in $\bar{p}p$ interactions in the midrapidity region from the Gaussian fit.

(9) The ratio of the invariant x distribution of $\pi^{\pm}$ mesons in pp interactions to the same distribution of $\pi^{\pm}$'s in $\bar{p}p$ interactions is ≈ 0.72 for $|x| < 0.45$.

(10) The invariant P_T^2 distributions of charged mesons in pp and $\bar{p}p$ interactions are well approximated by the transverse mass dependence with the slope parameter $T \approx m_\pi$.

(11) The quark-gluon string model (QGSM) reproduces the inclusive distributions of charged particles in both experiments rather well.

TABLE XIII. The results of the fit of inclusive and semi-inclusive $d\sigma/dP_T^2$ distributions of charged particles from pp and $\bar{p}p$ interactions at 32 GeV/c in the interval $0 < P_T^2 < 2$ (GeV/c)^2 to expression (34).

Multiplicity	A [mb/(GeV/c)^2]	B [(GeV/c)$^{-2}$]	n	χ^2/N_{DF}
$pp \to p + X$				
2 pr.	26.93± 0.76	31.49± 3.06	1.10± 0.03	255.01/18
4 pr.	61.47± 1.46	52.08± 4.71	0.96± 0.03	84.08/19
6 pr.	31.72± 1.08	16.01± 1.81	1.25± 0.01	82.22/19
8 pr.	16.68± 0.78	4.16± 0.48	2.17± 0.11	45.56/17
All	127.79± 2.27	24.27± 1.52	1.11± 0.02	232.21/19
$\bar{p}p \to \bar{p} + X$				
2 pr.	16.41± 0.48	46.46± 5.23	1.15± 0.05	24.33/18
4 pr.	29.79± 0.97	34.64± 3.98	1.06± 0.04	56.77/18
6 pr.	17.18± 0.83	17.14± 2.72	1.19± 0.07	42.49/18
8 pr.	6.10± 0.54	5.18± 1.40	2.07± 0.27	11.98/17
All	67.67± 1.69	17.68± 1.44	1.36± 0.04	121.51/19
$pp \to \pi^+ + X$				
2 pr.	38.25± 0.98	34.04± 4.38	1.87±0.13	16.88/16
4 pr.	147.23± 2.31	142.62± 8.05	0.96±0.02	123.69/18
6 pr.	157.30± 2.23	112.12± 5.65	1.09±0.02	170.70/19
8 pr.	97.37± 1.88	127.48± 8.31	1.14±0.02	102.18/19
10 pr.	37.32± 1.30	142.59±16.81	1.14±0.04	19.73/17
All	470.98± 4.16	100.78± 3.02	1.17±0.01	318.39/19
$\bar{p}p \to \pi^+ + X$				
2 pr.	31.01± 0.26	38.11± 6.24	1.84±0.20	18.00/14
4 pr.	127.86± 1.89	91.30± 5.18	1.15±0.02	209.18/16
6 pr.	164.52± 1.84	92.51± 3.69	1.13±0.02	340.70/17
8 pr.	132.33± 1.77	121.29± 5.51	1.07±0.01	227.68/17
10 pr.	71.37± 1.37	117.30± 7.61	1.13±0.02	118.37/16
All	527.78± 3.50	77.44± 1.70	1.27±0.01	546.37/18
$pp \to \pi^- + X$				
4 pr.	62.55± 2.71	82.93±20.97	1.11±0.07	540.28/19
6 pr.	113.52± 1.25	99.23± 3.15	1.13±0.01	343.19/19
8 pr.	77.26± 1.13	105.21± 4.30	1.19±0.01	231.02/18
10 pr.	34.06± 0.90	140.42± 9.95	1.20±0.02	95.01/16
All	313.38± 2.14	106.12± 2.19	1.13±0.01	570.47/21
$pp \to K^- + X$				
All	8.50 ± 4.27	144.81±177.70	0.773± 0.189	0.37/7

ACKNOWLEDGMENTS

We wish to express our gratitude to the technical staff associated with the MIRABELLE bubble chamber program at Serpukhov and at NPI MSU for their excellent work at the various stages of the experiment. Two of us (B.L.V. and Z.E.E.) wish to thank the International Office and Physics Department of the University of Bergen (Norway) for the financial support and the warm and kind hospitality.

APPENDIX: STATISTICAL METHOD FOR SEPARATION OF THE INCLUSIVE CHARGED PARTICLE SPECTRA IN pp AND $\bar{p}p$ COLLISIONS

The following technique for deriving charged particle spectra is an adaptation for pp interactions of the one generally used in $\bar{p}p$ collisions [14,15]. For pp interactions, a basically similar method has been used for the separation of p and π^+ spectra in [9,11]. Neglecting any information on particle identification, these methods take into account only charge identification and momentum measurements of particle tracks. Both of them are based on the fact that particle spectra in pp and $\bar{p}p$ interactions should obey charge conjugation symmetry. Thus, for pp collisions the spectra are forward-backward symmetric in the c.m.s. and for $\bar{p}p$ collisions the c.m.s. spectrum of a particle is identical with the reflected spectrum of its antiparticle or, in other words, a particle spectrum in the laboratory (target) frame is identical with the corresponding antiparticle spectrum in the projectile frame [14]. So, in the case of mass misidentification, the charge conjugation symmetry of charged particle and antiparticle spectra will fail.

The method described below is a generalization which includes both schemes previously discussed. It is also original, in the sense that it allows one to separate the kaon spectra as well as those of protons and pions.

Following the notation of [11,14], let us define the Lorentz-like transformations acting on longitudinal momentum q of a secondary particle:

$R_p : q \rightarrow R_p q$, Lorentz transformation from the target frame to the projectile frame (or vice versa) under

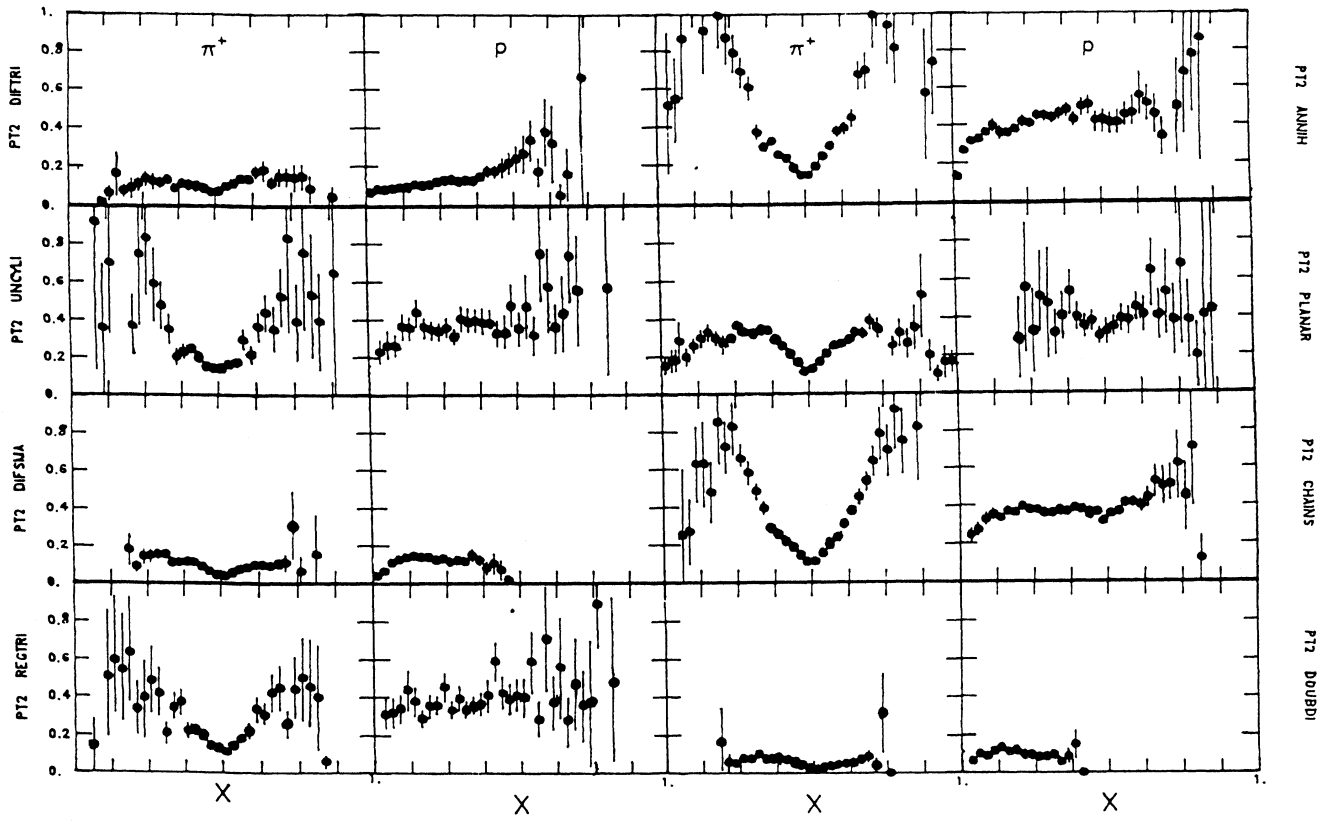

FIG. 33. The predictions of x dependence of $\langle P_T^2 \rangle$ for different QGSM diagrams in $\bar{p}p$ interactions at 32 GeV/c.

TABLE XIV. The results of the fit of inclusive and semi-inclusive $d\sigma/dP_T^2$ distributions of charged particles from pp and $\bar{p}p$ interactions at 32 GeV/c in the interval $0 < P_T^2 < 2$ (GeV/c)^2 to expression (35).

Multiplicity	A [mb/(GeV/c)$^{1/2}$]	T (GeV)	$\chi^2/N_{\rm DF}$
$pp \to p + X$			
2 pr.	$0.47\times10^5\pm1.1\times10^4$	0.097± 0.002	136.40/19
4 pr.	$3.00\times10^5\pm5.2\times10^4$	0.087± 0.001	69.16/20
6 pr.	$2.09\times10^4\pm3.9\times10^3$	0.111± 0.002	34.26/20
8 pr.	$4.68\times10^5\pm1.4\times10^5$	0.083± 0.002	22.77/18
10 pr.	$2.97\times10^4\pm3.0\times10^3$	0.111± 0.001	9.42/18
All	$1.51\times10^5\pm6.3\times10^3$	0.103± 0.002	79.65/20
$\bar{p}p \to \bar{p} + X$			
2 pr.	$5.35\times10^5\pm1.0\times10^3$	0.073± 0.060	34.74/19
4 pr.	$7.80\times10^4\pm2.1\times10^3$	0.093± 0.009	31.45/19
6 pr.	$1.09\times10^4\pm1.2\times10^3$	0.111± 0.053	27.29/19
8 pr.	$8.07\times10^3\pm3.3\times10^3$	0.104± 0.005	9.79/18
10 pr.	$1.37\times10^3\pm2.6\times10^3$	0.113± 0.031	10.43/18
All	$1.51\times10^5\pm2.4\times10^4$	0.097± 0.002	76.95/20
$pp \to \pi^+ + X$			
2 pr.	64.08 ± 1.86	0.119± 0.002	119.30/17
4 pr.	197.14 ± 3.34	0.128± 0.001	53.29/19
6 pr.	222.36 ± 3.53	0.124± 0.001	32.23/20
8 pr.	142.36 ± 3.20	0.116± 0.001	18.80/20
10 pr.	55.86 ± 2.38	0.110± 0.002	10.67/18
All	677.99 ± 6.77	0.122± 0.001	43.95/20
$\bar{p}p \to \pi^+ + X$			
2 pr.	43.58 ± 0.60	0.127± 0.002	140.12/15
4 pr.	183.27 ± 2.87	0.126± 0.001	64.72/17
6 pr.	235.92 ± 2.84	0.127± 0.001	60.09/18
8 pr.	186.83 ± 2.73	0.123± 0.001	24.72/18
10 pr.	105.46 ± 2.22	0.117± 0.001	12.01/17
All	786.42 ± 5.69	0.123± 0.001	67.91/19
$pp \to \pi^- + X$			
4 pr.	110.84 ± 1.38	0.129± 0.001	44.08/20
6 pr.	161.69 ± 1.87	0.125± 0.001	51.93/20
8 pr.	114.72 ± 1.80	0.118± 0.001	36.41/19
10 pr.	51.53 ± 1.57	0.108± 0.015	28.49/17
All	449.45 ± 3.34	0.122± 0.004	68.59/22
$pp \to K^- + X$			
All	50.72 ±59.80	0.134± 0.094	1.96/8

TABLE XV. The values of $\langle P_T\rangle$, $\langle P_T^2\rangle$, and the dispersion D of the charged particle P_T distributions. Of each pair of numbers, the upper one is for pp and the lower one is for $\bar{p}p$ interactions.

Particle	$\langle P_T\rangle$ (GeV/c)	$\langle P_T^2\rangle$ [(GeV/c)^2]	D (GeV/c)
π^+	0.333 ± 0.003	0.160± 0.003	0.222± 0.004
	0.331 ± 0.002	0.157± 0.002	0.219± 0.003
π^-	0.324 ± 0.003	0.152± 0.003	0.217± 0.004
	0.333 ± 0.002	0.158± 0.002	0.217± 0.003
p	0.465 ± 0.005	0.282± 0.005	0.256± 0.005
	0.461 ± 0.004	0.279± 0.004	0.258± 0.005
$\bar{p}$	-	-	-
	0.468 ± 0.004	0.284± 0.004	0.255± 0.005
K^-	0.428 ± 0.055	0.290± 0.061	0.327± 0.070
	-	-	-

TABLE XVI. Approximations of the average transverse momentum of charged particles from pp and $\bar{p}p$ interactions at 32 GeV/c at given parameter T.

Particle	Boltzmann	exp($-m_T/T$)	Hydrodyn.
p_{pp}	0.369±0.002	0.507±0.003	0.218±0.002
$\bar{p}_{\bar{p}p}$	0.358±0.002	0.486±0.003	0.206±0.002
π^+_{pp}	0.180±0.002	0.469±0.003	0.259±0.002
$\pi^+_{\bar{p}p}$	0.181±0.002	0.472±0.003	0.261±0.002
π^-_{pp}	0.180±0.002	0.469±0.003	0.259±0.002
K^-_{pp}	0.305±0.210	0.548±0.410	0.284±0.190

the assumption of proton mass plus reflection (changing the sign of momentum) along the longitudinal momentum axis.

$R_{\pi,K} : q \to R_{\pi,K}q$, the same transformation as R_p but assuming the pion and/or kaon mass for the track.

These definitions mean that

$$\begin{aligned} R_p &= \gamma(\beta\sqrt{q^2+r^2+m_p^2} - q), \\ R_\pi &= \gamma(\beta\sqrt{q^2+r^2+m_\pi^2} - q), \\ R_K &= \gamma(\beta\sqrt{q^2+r^2+m_K^2} - q), \end{aligned} \tag{A1}$$

where r^2 is the transverse momentum squared and γ and β are the Lorentz transformation factors,

$$\gamma = E_{\text{beam}}/m_p \quad , \quad \beta = P_{\text{beam}}/E_{\text{beam}} . \tag{A2}$$

The differential cross sections of particles $d\sigma$ can be denoted as f, and so $d\sigma(p) \equiv f_p$, $d\sigma(\pi^+) \equiv f_{\pi^+}$, etc. From the definition (A1) of the R_x operators and from the forward-backward symmetry for pp interactions, the following relations should be valid:

$$\begin{aligned} R_p f_p &= f_p, \\ R_\pi f_{\pi^\pm} &= f_{\pi^\pm}, \\ R_K f_{K^\pm} &= f_{K^\pm} . \end{aligned} \tag{A3}$$

Similarly, using the charge conjugation symmetry for $\bar{p}p$ collisions one can write

$$\begin{aligned} R_p f_p &= f_{\bar{p}}, \\ R_p f_{\bar{p}} &= f_p, \\ R_\pi f_{\pi^\pm} &= f_{\pi^\mp}, \\ R_K f_{K^\pm} &= f_{K^\mp} . \end{aligned} \tag{A4}$$

The separation methods mentioned above in principle did not involve more than two different particle spectra, respectively, for the positive and negative parts of the whole sample of particles. For instance, they permit to separate only $(\bar{p}, \pi^-)$ and (p, π^+) in $\bar{p}p$ interactions [14,15]. Including the third possible particle in secondaries spectrum is extremely difficult. A method for deriving $K^\pm$ spectra in $\bar{p}p$ interactions was first proposed in [3], but it is rather complicated. Therefore, the separation problem should be subdivided into two parts: (a) separation of four different particle spectra (2+2) both in pp and $\bar{p}p$ collisions; (b) further development of the algorithm in order to separate six (3+3) particle spectra.

1. Separation of p, $\pi^\pm$, and K^- spectra in pp collisions

In this case, the positive and negative parts of the whole spectrum of secondaries can be defined as

$$f_+ = f_p + f_{\pi^+} \quad , \quad f_- = f_{K^-} + f_{\pi^-} . \tag{A5}$$

In order to demonstrate this algorithm in detail, let us obtain a recurrent formula for extracting π^-. Using the relations (A3) for the $R_{\pi,K}$ operators, one can rewrite the second equation of (A5) in the form

$$\begin{aligned} f_{\pi^-} &= f_- - R_K f_{K^-} = f_- - R_K(f_- - f_{\pi^-}) \\ &= f_- - R_K(f_- - R_\pi f_{\pi^-}) \\ &= f_- - R_K f_- + R_K R_\pi f_{\pi^-} . \end{aligned} \tag{A6}$$

For other particles similar recurrent equations will be

$$f_{K^-} = f_- - R_\pi f_- + R_\pi R_K f_{K^-}, \tag{A7}$$

$$f_p = f_+ - R_\pi f_+ + R_\pi R_p f_p, \tag{A8}$$

$$f_{\pi^+} = f_+ - R_p f_+ + R_p R_\pi f_{\pi^+} . \tag{A9}$$

How can these equations be applied for spectra separation? For instance, if a particle has negative charge, then

$$\begin{aligned} f_{\pi^-}^{(0)} &= f_- - R_K f_-, \\ f_{\pi^-}^{(1)} &= R_K R_\pi f_{\pi^-}^{(0)}, \\ &\vdots \\ f_{\pi^-}^{(n+1)} &= R_K R_\pi f_{\pi^-}^{(n)}, \\ &\vdots \\ f_{\pi^-} &= f_{\pi^-}^{(0)} + f_{\pi^-}^{(1)} + \cdots + f_{\pi^-}^{(n)} + \cdots . \end{aligned} \tag{A10}$$

In principle, this algorithm creates an infinite series of operator chains like $R_\pi R_K R_\pi R_K \cdots$, but using the fact that

$$R_\pi R_\pi q = q \ , \ R_K R_K q = q \ , \tag{A11}$$

it is easy to prove that the inequalities

$$R_\pi R_K q < q < R_K R_\pi q \tag{A12}$$

hold for any q (and r) [14]. Thus, it is necessary to compute only those transformed momenta, which do not leave the region allowed by kinematics. In the case of the energy in question, the average number of iterations like (A10) was about 8–9 and the upper limit was 30.

It is necessary to mention an important point in this scheme. Let us return to Eq. (A6). One can act on both the left-hand side (LHS) and RHS of this equation by the operator R_π:

$$R_\pi f_{\pi^-} = R_\pi f_- - R_\pi R_K f_- + R_\pi R_K R_\pi f_{\pi^-} . \tag{A13}$$

Finally, according to definition $R_\pi f_{\pi^-} = f_{\pi^-}$,

$$f_{\pi^-} = R_\pi f_- - R_\pi R_K f_- + R_\pi R_K R_\pi f_{\pi^-} . \tag{A14}$$

In this case, first the boost from the laboratory frame to the projectile one was used. Then, after the momentum reflection along the longitudinal momentum axis, the algorithm described above was applied to the "reflected" spectra. Why is this important? In practice, the spectra of secondary particles derived by the above operators are slightly inaccurate statistically due to systematics. For example, they are nonsymmetric in the backward-forward hemispheres. Thus the combination of the two spectra, "direct" and "reflected," will provide statistically more accurate results.

2. Separation of p, $\pi^{\pm}$, and $\bar{p}$ spectra in $\bar{p}p$ collisions

In the case of antiproton-proton collisions, one can write, for the positive and negative parts of the secondary particle spectrum,

$$f_+ = f_p + f_{\pi^+} \quad , \quad f_- = f_{\bar{p}} + f_{\pi^-}, \tag{A15}$$

and, together with the expressions (A4) for the transformation operators, a set of recurrent formulas like (A6)–(A9) can be derived as

$$f_p = f_+ - R_\pi f_- + R_\pi R_p f_p, \tag{A16}$$
$$f_{\pi^+} = f_+ - R_p f_- + R_p R_\pi f_{\pi^+}, \tag{A17}$$
$$f_{\pi^-} = f_- - R_p f_+ + R_p R_\pi f_{\pi^-}, \tag{A18}$$
$$f_{\bar{p}} = f_+ - R_\pi f_+ + R_\pi R_p f_{\bar{p}} . \tag{A19}$$

Comparing Eqs. (A16)–(A19) to (A6)–(A9), it is easy to notice the main difference between them. Because of forward-backward symmetry of c.m.s. spectra in pp interactions one is able to derive positive secondaries independently from the negative ones, while because of charge conjugation symmetry in the $\bar{p}p$ collisions, one has to take into account both the positive and negative parts of the total spectrum in order to reconstruct any inclusive single-particle distribution.

It can be noticed also that it is unnecessary to introduce different operators acting only on positive or on negative particles [14].

Modification of this technique for including the third particle in positive or negative spectra of secondaries first was discussed in [4]. In this report a number of difficulties for searching for a suitable three-particle algorithm was pointed out. Now we would like to present one of the possible solutions of the problem.

3. Separation of kaon spectra in pp and $\bar{p}p$ collisions

The problem of K^+ spectrum separation in pp interactions will be discussed first. Here, for the positive part of the spectrum of secondaries,

$$f_+ = f_p + f_{\pi^+} + f_{K^+}, \tag{A20}$$

and, using (A3),

$$f_p = f_+ - R_\pi f_+ - R_K f_+ + R_\pi R_p f_p + R_K R_p f_p + R_\pi R_K f_{K^+} + R_K R_\pi f_{\pi^+}, \tag{A21}$$
$$f_{\pi^+} = f_+ - R_p f_+ - R_K f_+ + R_p R_\pi f_{\pi^+} + R_K R_\pi f_{\pi^+} + R_p R_K f_{K^+} + R_K R_p f_p, \tag{A22}$$
$$f_{K^+} = f_+ - R_p f_+ - R_\pi f_+ + R_p R_K f_{K^+} + R_\pi R_K f_{K^+} + R_p R_\pi f_{\pi^+} + R_\pi R_p f_p, \tag{A23}$$

and so instead of (A10) a much more complicated chain of recurrent equations should be considered:

$$\begin{aligned}
f_{\pi^+} &= f_{\pi^+}^{(0)} + f_{\pi^+}^{(1)} + \cdots + f_{\pi^+}^{(n)} + \cdots, \\
f_{K^+} &= f_{K^+}^{(0)} + f_{K^+}^{(1)} + \cdots + f_{K^+}^{(n)} + \cdots, \\
f_p &= f_p^{(0)} + f_p^{(1)} + \cdots + f_p^{(n)} + \cdots, \\
f_{\pi^+}^{(0)} &= f_+ - R_K f_+ - R_p f_+, \\
f_{K^+}^{(0)} &= f_+ - R_\pi f_+ - R_p f_+, \\
f_p^{(0)} &= f_+ - R_\pi f_+ - R_\pi f_+, \\
&\vdots \\
f_{\pi^+}^{(n+1)} &= (R_p R_\pi + R_K R_\pi) f_{\pi^+}^{(n)} + R_p R_K f_{K^+}^{(n)} + R_K R_p f_p^{(n)}, \\
f_{K^+}^{(n+1)} &= (R_p R_K + R_\pi R_K) f_{K^+}^{(n)} + R_p R_\pi f_{\pi^+}^{(n)} + R_\pi R_p f_p^{(n)}, \\
f_p^{(n+1)} &= (R_K R_p + R_\pi R_p) f_p^{(n)} + R_\pi R_K f_{K^+}^{(n)} + R_K R_\pi f_{\pi^+}^{(n)} .
\end{aligned} \tag{A24}$$

Including $K^{\pm}$ - spectra for $\bar{p}p$ interaction case will lead to the equations

$$f_{p/\bar{p}} = f_\pm - R_\pi f_\mp - R_K f_\mp (R_\pi R_p + R_K R_p) f_{p/\bar{p}} + R_\pi R_K f_{K^\pm} + R_K R_\pi f_{\pi^\pm}, \tag{A25}$$
$$f_{\pi^\pm} = f_\pm - R_p f_\mp - R_K f_\mp + (R_p R_\pi + R_K R_\pi) f_{\pi^\pm} + R_p R_K f_{K^\pm} + R_K R_p f_{p/\bar{p}}, \tag{A26}$$
$$f_{K^\pm} = f_\pm - R_p f_\mp - R_\pi f_\mp + (R_p R_K + R_\pi R_K) f_{K^\pm} + R_p R_\pi f_{\pi^\pm} + R_\pi R_p f_{p/\bar{p}} ; \tag{A27}$$

thus,

$$\begin{aligned}
f_{\pi^\pm}^{(0)} &= f_\pm - R_K f_\mp - R_p f_\mp, \\
f_{K^\pm}^{(0)} &= f_\pm - R_\pi f_\mp - R_p f_\mp, \\
f_{p/\bar{p}}^{(0)} &= f_\pm - R_\pi f_\mp - R_\pi f_\mp, \\
&\vdots
\end{aligned} \tag{A28}$$

$$f_{\pi^\pm}^{(n+1)} = (R_p R_\pi + R_K R_\pi) f_{\pi^\pm}^{(n)} + R_p R_K f_{K^\pm}^{(n)} + R_K R_p f_{p/\bar{p}}^{(n)},$$
$$f_{K^\pm}^{(n+1)} = (R_p R_K + R_\pi R_K) f_{K^\pm}^{(n)} + R_p R_\pi f_{\pi^\pm}^{(n)} + R_\pi R_p f_{p/\bar{p}}^{(n)},$$
$$f_{p/\bar{p}}^{(n+1)} = (R_K R_p + R_\pi R_p) f_{p/\bar{p}}^{(n)} + R_\pi R_K f_{K^\pm}^{(n)} + R_K R_\pi f_{\pi^\pm}^{(n)} .$$

It is easy to see from (A10) that any term in the infinite series expansion can be calculated by acting with only one operator combination, for example, $R_\pi R_p$, on the previous term, and so there is no increase of terms at any step of the iteration. Formally, applying this algorithm to (A24), (A28) will give rise to a number of terms like a geometrical progression with a factor of 4 in accordance with the number of coupling operators. In that case one should use an enormously large amount of computer memory and the algorithm might be useful for the collisions at not very high energies only (less than 5–7 GeV/c). Consequently, the question is, can the three-particle method be helpful for higher energies or not? One of the possible solutions is to generate the chain of operators acting on the zeroth-order terms in (A24) or (A28). To clarify this idea let us show the second-order term in expansion for the p spectrum [in that case, it does not matter for pp or $\bar{p}p$ interactions the problem will be solved, because the difference between these two cases is contained in zeroth-order terms according to (A24) or (A28)]. Thus,

$$\begin{aligned} f_p^{(2)} = {} & (R_\pi R_p R_\pi R_p + R_\pi R_p R_K R_p + R_K R_p R_\pi R_p + R_K R_p R_K R_p + R_\pi R_K R_\pi R_p + R_K R_\pi R_K R_p) f_p^{(0)} \\ & + (R_\pi R_p R_\pi R_K + R_K R_p R_\pi R_K + R_\pi R_K R_p R_K + R_\pi R_K R_\pi R_K + R_K R_\pi R_p R_K) f_K^{(0)} \\ & + (R_\pi R_p R_K R_\pi + R_K R_p R_K R_\pi + R_\pi R_K R_p R_\pi + R_K R_\pi R_p R_\pi + R_K R_\pi R_K R_\pi) f_\pi^{(0)} . \end{aligned} \tag{A29}$$

The rules for constructing the operator chains may be formulated as follows.

Operator R_i can act only on the $f_i^{(0)}$ term (R_p on $f_p^{(0)}$, R_π on $f_{\pi^\pm}$, etc.). Operator R_i cannot occupy the first position in any chain in an expression for $f_i^{(n)}$ [for example, there is no R_p operator at the first place in any operator groups in (A29)].

It is forbidden for the identical operators to be together inside the operator chain (i.e., combinations like $R_\pi R_p R_p R_K$ do not exist).

For an nth-order term the corresponding operator chains will consist of $2n$ different operators of R_i type.

This algorithm does not need large computer memory. Instead of memory (i.e., space) it demands a lot of CPU time which, in principle, cannot be considered as a crucial restriction because of the continual increase of computer facilities.

[1] A. B. Kaidalov, Phys. Lett. **116B**, 459 (1982); A. B. Kaidalov and K. A. Ter-Martirosyan, **117B**, 247 (1982); Sov. J. Nucl. Phys. **39**, 979 (1984); A. B. Kaidalov, *ibid.* **45**, 902 (1987).

[2] N. S. Amelin, L. V. Bravina, L. I. Sarycheva, and L. N. Smirnova, Sov. J. Nucl. Phys. **50**, 1058 (1989); N. S. Amelin and L. V. Bravina, *ibid.* **51**, 133 (1990).

[3] E. V. Vlasov *et al.*, Z. Phys. C **13**, 95 (1982).

[4] L. V. Bravina, E. E. Zabrodin, and N. A. Kruglov, Report No. NPI MSU 90-43/189, 1990 (unpublished).

[5] L. V. Bravina *et al.*, Sov. J. Nucl. Phys. **46**, 1002 (1987).

[6] M. A. Jabiol *et al.*, Nucl. Phys. **B127**, 365 (1977).

[7] C. Poiret *et al.*, Z. Phys. C **11**, 1 (1981).

[8] L. V. Bravina *et al.*, Report No. NPI MSU 90-44/190, 1990 (unpublished).

[9] D. B. Smith *et al.*, Phys. Rev. Lett. **23**, 1064 (1969).

[10] V. Blobel *et al.*, Nucl. Phys. **B69**, 454 (1974).

[11] V. Idschok *et al.*, Nucl. Phys. **B67**, 93 (1973).

[12] V. V. Ammosov *et al.*, Nuovo Cimento **40**, 237 (1977).

[13] C. P. Ward *et al.*, Nucl. Phys. **B153**, 299 (1979).

[14] P. Johnson *et al.*, Nucl. Phys. **B173**, 77 (1980).

[15] E. G. Boos *et al.*, Nucl. Phys. **B121**, 381 (1977); **B174**, 45 (1980).

[16] H. U. Bengtsson and G. Ingelman, Comput. Phys. Commun. **34**, 251 (1985).

[17] B. Andersson, G. Gustafson, and X. Nilsson-Almqvist, Nucl. Phys. **B281**, 289 (1987).

[18] N. S. Amelin *et al.*, Report No. NPI MSU 89-55/132, 1989 (unpublished).

[19] G. Veneziano, Phys. Lett. **52B**, 220 (1974).

[20] A. Capella and J. Tran Thanh Van, Phys. Lett. **93B**, 146 (1980); **114B**, 450 (1982).

[21] A. Capella and J. Tran Thanh Van, Z. Phys. C **18**, 85 (1983).

[22] P. E. Volkovitsky, Sov. J. Nucl. Phys. **43**, 171 (1986).

[23] R. D. Field and R. P. Feynman, Nucl. Phys. **B136**, 1 (1978).

[24] B. Hanumajh *et al.*, Nuovo Cimento A **68**, 161 (1982).

[25] C. N. Booth *et al.*, Phys. Rev. D **27**, 2018 (1983).

[26] S. J. Brodsky and J. F. Gunion, Phys. Rev. D **17**, 848 (1978).

[27] J. Rushbrooke and B. R. Webber, Phys. Rep. **44**, 1 (1978).

[28] H. G. Kirk and M. Matziolis, Lett. Nuovo Cimento **12**, 75 (1975).

[29] L. D. Landau, Izv. Acad. Nauk USSR **17**, 51 (1953).

[30] L. D. Landau and S. Z. Belenkij, Nuovo Cimento Suppl. **3**, 15 (1956).

[31] H. A. Milekhin, Sov. Phys. JETP **35**, 372 (1959).

[32] E. V. Shuryak, Yad. Fiz. **16**, 395 (1972) [Sov. J. Nucl. Phys. **16**, 220 (1973)].

[33] H. von Gersdorff, L. McLerran, M. Kataja, and P. V. Ruuskanen, Phys. Rev. D **34**, 794 (1986).

[34] R. P. Feynman, Phys. Rev. Lett. **23**, 1415 (1969).

[35] G. D. Patel *et al.*, Z. Phys. C **12**, 189 (1982).
[36] G. W. van Apeldorn *et al.*, Phys. Lett. **115B**, 55 (1982).
[37] B. V. Batyunja *et al.*, Report No. JINR 1-80-326, 1980 (unpublished).
[38] R. M. Robertson *et al.*, Phys. Rev. D **21**, 3064 (1980).
[39] L. V. Bravina *et al.*, Sov. J. Nucl. Phys. **43**, 574 (1986).
[40] B. V. Batyunja *et al.*, Report No. JINR 1-84-779, 1984 (unpublished).
[41] M. Yu. Bogolyubskii *et al.*, Sov. J. Nucl. Phys. **50**, 424 (1989).
[42] P. V. Landshoff and J. C. Polkinghorne, Phys. Lett. **45B**, 361 (1973).
[43] M. K. Chase and M. J. Stirling, Nucl. Phys. **B133**, 157 (1978).
[44] M. Yu. Bogolyubskii *et al.*, Sov. J. Nucl. Phys. **47**, 455 (1988).
[45] R. Hagedorn, Riv. Nuovo Cimento **6**, 1 (1983).
[46] J. Schukraft, Report No. CERN-PPE/91-04, 1991 (unpublished).
[47] R. Hagedorn and J. Rafelski, Phys. Lett. **97B**, 136 (1980).
[48] J. P. Blaizot and J. Y. Ollitrault, in *Quark-Gluon Plasma*, edited by R. C. Hwa, Advanced Series on Directions in High Energy Physics Vol. 6 (World Scientific, Singapore, 1990), p. 393.